Journal of Structural Geology, Vol. 15, No. 1, pp. 1 to 20, 1993
Printed in Great Britain

0191-8141/93 $06.00+0.00
Pergamon Press Ltd

Strain and kinematic analysis in general shear zones

CAROL SIMPSON*

Division of Earth Sciences, National Science Foundation, Washington, DC 20550, U.S.A.

and

DECLAN G. DE PAOR

Department of Earth and Planetary Sciences, The Johns Hopkins University, Baltimore, MD 21218, U.S.A.

(*Received* 12 *December* 1991; *accepted in revised form* 21 *May* 1992)

Abstract—We present a unifying theory for the development and distribution of strain markers and kinematic indicators in zones of general shear, and thus provide a framework in which data previously considered contradictory may be understood. Rigid and deformable porphyroclast systems, including σ, δ and complex σ–δ grains are potential indicators of both strain and flow. The shapes and distribution of such porphyroclast systems may be used to distinguish among different tectonic regimes.

General shear is divided into two fields: sub-simple shear, in which the rotational component of the strain is less than that for simple shear, and super-simple shear, in which the rotational component is greater than for simple shear. Sub-simple shear may involve narrowing or broadening of shear zones. Super-simple shear regimes are possible in local regions such as the vicinities of deformable porphyroclasts, but must be enclosed by regimes of sub-simple shear.

The polar Mohr constructions for finite deformation and flow are useful to analyze general shear in theory. The hyperbolic net is employed for practical plotting of real data and derivation of the kinematic vorticity number, W_n. This number represents the relative contributions of pure and simple shear in steady flow. In nature, deformation is thought to build up and decay by processes that may invalidate the assumption of constant flow regime. We therefore introduce the concept of accelerating deformation and analyze the implications of non-steady flow for the shearing histories of deformed objects.

INTRODUCTION

STRUCTURAL geologists possess a variety of tools for the strain and kinematic analysis of deformed rocks. However, few workers have been able to quantify deformation states and paths in the same rocks, partly owing to the nature of the materials involved. Finite strain is easy to measure in low-grade rocks containing linear or angular markers that obey the March model (1932), or elliptical objects such as reduction spots (Ramsay 1967), but such rocks rarely contain a record of the strain path. To develop incremental strain markers such as fibrous beards on pebbles, relatively rigid objects are required, but such objects do not accurately record finite strain. Rotated structures such as dynamically recrystallized porphyroclasts are common in high strain mylonites with a strong fabric (Simpson & Schmid 1983, Hanmer & Passchier 1991), but these rocks often lack cumulative or even incremental strain markers. As pointed out by Passchier (1986) and re-emphasized by Choukroune *et al.* (1987), the quantitative relations between non-coaxiality and structural asymmetry have remained uncertain. Furthermore, theoretical relationships between deformation state and path have been obscured in the past by measurement in different reference frames. Finite strains were traditionally plotted on quadratic Mohr diagrams (usually labelled λ, γ or λ', γ'), whereas infinitesimal extensions ε were plotted against engineer's shear strain $\gamma/2$.

In this work, deformation refers to the transformation of material from one geometric or mechanical state to another and shear refers to any deformation that changes the angles between intersecting lines. Finite and infinitesimal strains are both represented more simply in terms of stretch S, extension ε, and shear strain γ, and the relationship between deformation state and path is clarified. We show how strain markers, fabric elements and objects traditionally used as simple shear sense indicators are more easily explained by general shear in a high strain zone. In addition, these markers yield information about the velocity gradients leading to that state of general shear, and the accelerations involved in the waxing and waning stages of the flow.

GENERAL SHEAR

Deformation state

Since the early work of Sorby (1855), Harker (1885) and Wettstein (1886) structural geologists have tended to rely on three simplistic deformation models: pure shear, simple shear and rigid rotation. These terms have strict definitions in classical mechanics but are used more casually in structural geology. Pure shear is used to

*Also at: Department of Earth and Planetary Sciences, The Johns Hopkins University, Baltimore, MD 21218, U.S.A.

denote any deformation whose three principal stretching directions are eigenvectors (directions of no rotation). Simple shear is a deformation whose eigenvectors are confined to a plane—the shear plane. For rigid rotation, there is just one eigenvector—the rotation axis.

Ramsay & Graham (1970) demonstrated that simple shear is the only constant volume strain regime that can occur in straight, parallel-sided shear zones bounded by undeformed wall rocks unless there is a discontinuity (fault) along the boundary. More general deformation states were first discussed by Ramsay & Wood (1973) and Sanderson (1976), who examined the superposition of plane strain on an initial uniaxial compaction. Matthews *et al.* (1974) factorized deformation into pure shear and orthogonal simple shear along bedding planes. Other work on general deformation includes: curved shear zones (Coward 1976); dikes that intruded during combined shear and extension (Escher *et al.* 1975); non-coaxiality in progressive deformation (Means *et al.* 1980); and shear zones with non-parallel sides and terminations (Simpson 1983).

De Paor (1983) defined two fields of general shear—namely sub-simple shear, in which the rotational component of strain is less than that for the simple shear of the same intensity, and super-simple shear, in which the rotation is greater than for simple shear. Some authors ignore the latter category and use the term general shear for the former. Although super-simple shears are generally confined to special places such as the interiors of deformable porphyroclasts or regions of particulate flow, they may constitute an extremely important component of heterogeneous deformation regimes (Talbot & Jackson 1987).

Sub-simple shear zones may become narrower or broader. Reduction of a shear zone's thickness may be achieved by (a) increase in length, (b) reduction in volume, or (c) extension in the third dimension (i.e. transpression, Sanderson & Marchini 1984). In this paper we mainly consider the temporal evolution of a parallel-sided shear zone's profile plane, but much of the discussion may be applied to spatial gradients in shear zones that have non-parallel sides.

Mohr circle for strain

The Mohr circle construction for strain serves as a powerful tool for studying general shear. The traditional Mohr construction (Brace 1961) employed a quadratic λ', γ' reference frame and was limited to irrotational strains. The construction for strain introduced by De Paor (1983) is simple and very similar in principle to the well-known Mohr circles for stress. In the stress case, the *Cartesian* co-ordinates of each point on the circle represent the normal and shear stresses acting on a certain plane, whereas in De Paor's construction for strain the *polar* co-ordinates of a point on the circle represent the stretch and rotation of a certain line (Fig. 1a). For general strain in shear zones, the zone boundary is the baseline and the normal to the shear zone is then the polar co-ordinate reference axis or zero direction (Fig. 1b). In this reference frame, the shear zone boundary is clearly a direction of no rotation, i.e. an eigenvector. To construct the Mohr circle, the baseline stretch vector ξ_1 in geographical space is rotated through 90° and marked along the reference axis. This point has polar co-ordinates $(\xi_1, 0)$ in strain space. The deformed normal to the shear zone is marked at (S_0, ψ); being the only point representing a stretched line simultaneously in geographical space and strain space, it is termed the anchor point. The circle is drawn diametrically through $(\xi_1, 0)$ and (S_0, ψ) (Fig. 1b). In the special case of irrotational strain this circle's center falls on the reference axis.

The stretch and rotation of a particular material line are represented by a point (S, α) on the perimeter of the circle (Fig. 1c). Given this point, the corresponding line orientation in geographical space is obtained by pivoting the stretch vector about its second intersection with the circle until it passes through the anchor point (Fig. 1c). This gives the line's final orientation β' in geographical space. Its initial orientation β differs from β' by α, the rotation of the line.

The points on the circle that are furthest from and nearest to the origin represent the lines of maximum and minimum stretch, S_1 and S_2. They were initially 90° apart in geographical space and, having undergone equal rotations ω, they are also orthogonal after deformation; hence they have suffered no net shear strain (Fig. 1d). Any other pair of diametrically opposite points on the circle represents the stretch and rotation of a pair of initially orthogonal lines in geographical space and the angle they subtend at the origin is their angular shear ψ (Fig. 1e). Maximum angular shear is recorded by the pair of lines that were initially oriented symmetrically at ±45° to the principal directions (Fig. 1f). Their final orientations are indicated in Fig. 1(g). In Fig. 1(h) the two points where the circle intersects the reference axis represent the eigenvectors $(\xi_1, 0)$ and $(\xi_2, 0)$ of this general shear. The stretches ξ_1 and ξ_2 are the corresponding eigenvalues. The corresponding directions in geographic space are obtained by the pivoting manouver described above which yields the shear zone boundary and a second direction inclined in the displacement direction (Fig. 1h). Note that this figure illustrates the case of a narrowing sub-simple shear zone. In the opposite case of a broadening zone, the eigenvalue ξ_1 would be less than ξ_2.

Different sign conventions for Mohr constructions are advocated by various authors (see summary in Allison 1984). There are eight possible choices of sign convention; we prefer the one described above because: (1) it reduces the construction steps to a minimum; (2) the anchor point links strain space to geographic space; (3) rotational strains are measured in the same sense in strain space and geographical space; and (4) stretches and rotations of lines are referred to the final state preserved in the rock. By comparison, the polar co-ordinates of Means' (1982, 1983) construction are the stretch and the negative of the rotation of a line. His circle's pole, which plots diametrically opposite our

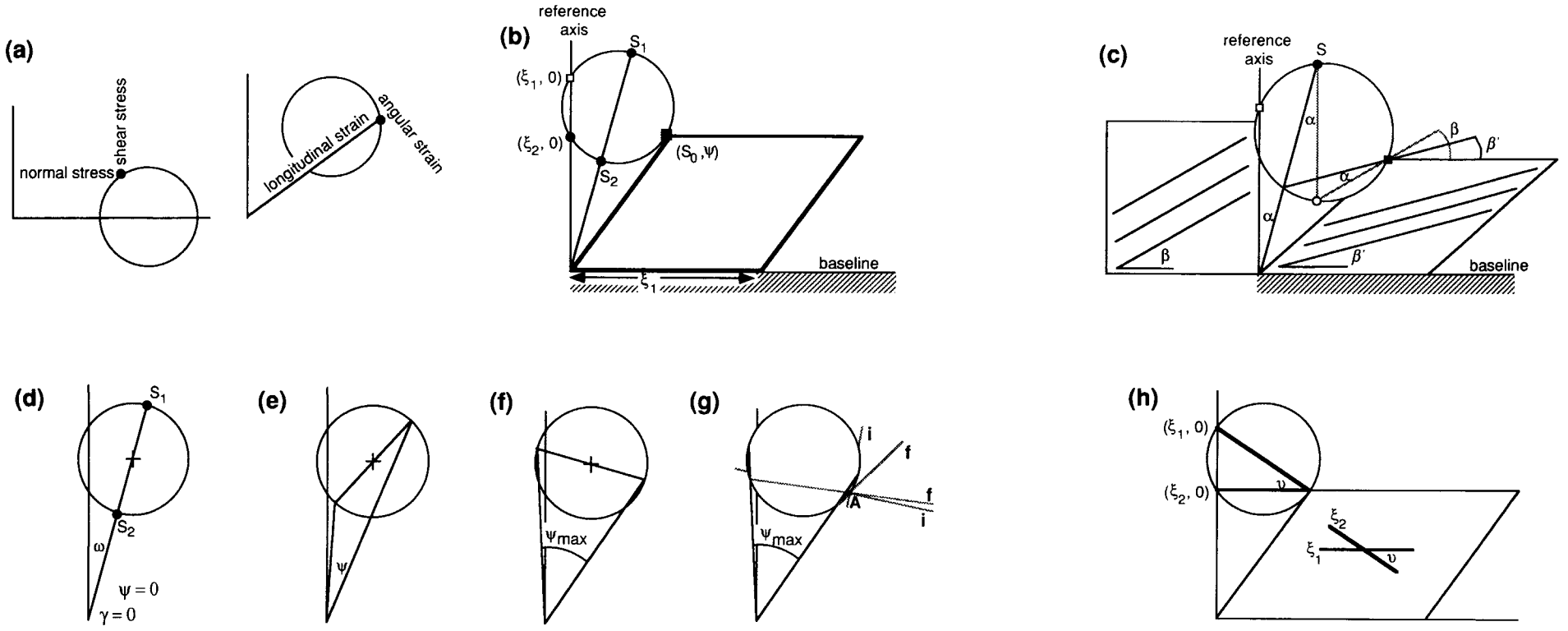

Fig. 1. Explanation of construction for strain. (a) Traditional Cartesian Mohr construction for stress, amd similar polar construction for strain. Vertical line is polar reference axis. (b) Baseline is shear zone boundary (shaded). Its normal is polar reference axis. Parallelogram represents deformed original square. ξ_1 is stretch of shear zone boundary; ξ_1,0 represents baseline in Mohr space. S_0 and ψ are stretch and rotation of pole to shear zone. Solid square is anchor point: it represents deformed pole to shear zone in real space and in Mohr space. ξ_2 is second eigenvalue. S_1 and S_2 are principal stretches. (c) Given point (S,α) on he Mohr circle, corresponding direction in real space is obtained by taking line through S and pivoting about its second intersect point on the Mohr circle (open circle) until it passes through anchor point (solid square). This is line's deformed orientation β'. Initial orientation is obtained by dashed construction lines. Sets of lines represent undeformed (dashed) and deformed (solid) directions. (d) Principal stretches S_1 and S_2 plot on circle's central axis. ω = rigid rotation; angular shear is zero. (e) Angular shear ψ is given by angle subtended at origin by any diametrically opposite pair of points. (f) Maximum ψ occurs when triangle is isosceles. (g) Construction for maximum shear γ_{max} (= tan ψ_{max}). Geographical directions as in (f). Initial directions, i, are perpendicular; final directions, f, are not. A = anchor point. Construction follows rules outlined in (c). (h) Lines of zero rotation in geographical space and Mohr space. ν is angle between eigenvectors. ξ_1, ξ_2 are corresponding eigenvalues.

anchor point, identifies the initial orientation of the corresponding direction in geographical space.

Deformation path

Deformation is a progressive phenomenon that follows a particular deformation path. The path is a closed loop in stress–strain space in the case of elastic behavior; alternatively an open-ended deformation path may lead either to fracture and rupture of the material, or to permanent strain. Ramberg (1975) derived particle paths for various combinations of coaxial and non-coaxial flow. Particle paths represent the cumulative changes in position of points during progressive deformation that is built up by identical increments of infinitesimal strain (Fig. 2). A consequence of this time invariance is that the displacement of a particle is a function of position only. When one particle reaches a position previously occupied by another, its displacement is identical to that of its predecessor. Ramberg (1975) showed that particle paths could be open-ended or form closed loops. Weijermars (1991) illustrated Ramberg's particle paths for the special case where stress and infinitesimal strain axes are coincident (i.e. where there is no material anisotropy).

Progressive stretch histories and rotations of lines

The stretching histories of lines during progressive shear are complex (Flinn 1962). Ramsay (1967) showed that lines oriented close to the S_1 direction may lengthen throughout their deformational history whereas lines close to the S_3 axis may shorten first and then lengthen. The rotation histories of lines during general shear are also complex. In progressive pure shear, material lines tend to rotate away from S_3 towards S_1, veering toward S_2 en route (Flinn 1962). Rotation increments are greatest at a high angle to all three principal directions and drop to zero along each principal direction. In sub-simple shear, there are two unequal fields of opposite rotation, bounded by the eigenvectors. Lines parallel to the eigenvectors do not rotate. Simple shear causes all material lines oblique to the flow plane to rotate toward the flow direction. One circular section of the simple shear strain ellipsoid is attached to the flow plane, the other begins perpendicular to it and progesssively rotates toward the flow direction. The long axis of the strain ellipsoid always bisects the acute angle between the circular sections, so it too rotates toward the flow direction.

The rate of rotation of lines increases with obliquity to the flow plane and reaches a maximum in the perpendicular plane. Once lines pass through this plane, their rate of rotation slows down so they approach but never reach the flow plane. The rotation rates of the strain ellipsoid axes also decelerate, although not as fast. In simple shear, material lines which lie along the S_1 and S_3 axes of the strain ellipsoid rotate faster than the strain ellipsoid axes; thus material constantly flows through two principal planes of the strain ellipsoid. After passing through the principal plane containing S_1, a material line's rotation rate is reduced and soon becomes slower than the rotation of the principal axes. Thus the angle subtended between a material line and the immaterial long axis of the strain ellipsoid passes through a maximum value and then reduces. The implications of this theoretical result for practical analysis of fabrics are significant. A small rigid elongate crystal will tend to grow fibrous tails as it rotates in progressive simple shear. These tails are deflected towards the S_1 direction and so their shape varies with time in a complex way. In super-simple shear, all lines rotate in the same sense but at different, pulsating rates.

Planes are rotated and deformed in a complex way during progressive deformation (March 1932, Owens 1973). Even in progressive pure shear, deformation involves rotation in any plane that is oblique to all three principal axes. Distortion is accompanied by rotation of the plane's pole and by spin about that pole. Even if volume is conserved, areas of oblique planes, which may be calculated using De Paor's (1983) tensor, are progressively altered. Some are shrunk, then restored, and finally spread beyond their initial area. Poles to planes of no area change form loci similar to directions of no longitudinal strain.

During shear deformation, lines oblique to the principal directions rotate out of orthogonality to their cross-sectional planes and thus become sheared. After a finite simple shear, some directions are sheared dextrally and others sinstrally (Fig. 3). Furthermore, during deformation some lines' shear strains progressively increase in magnitude whereas others decrease. Eventually, each sinistrally sheared line in a dextral shear zone attains a maximum shear value, reduces its shear strain to zero as

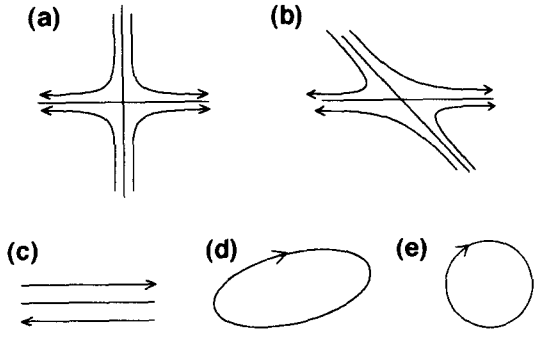

Fig. 2. Particle paths, after Ramberg (1975). (a) Pure shear, (b) sub-simple shear, (c) simple shear, (d) super-simple shear, (e) rigid rotation.

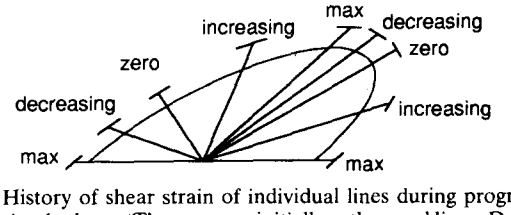

Fig. 3. History of shear strain of individual lines during progressive dextral simple shear. 'T's represent initially orthogonal lines. Depending on orientation, shear strain may be increasing or decreasing in current increment of deformation.

it passes through the long axis of the strain ellipsoid and then becomes sheared dextrally. Similarly, some dextrally sheared lines reduce their shear strain to zero as they pass through the short axis of the strain ellipsoid and then become sheared sinistrally. Thus it should not be surprising that individual kinematic indicators in a materially heterogeneous rock show shear sense opposite to the bulk shear direction. In progressive pure shear, the shear strain builds up continuously and monotonously; unlike the case of simple shear, there are no turning points in the magnitude of shear strain. For subsimple shear, there is one turning point. Shear strains pulsate for super-simple shear.

Mohr construction for infinitesimal strain

In the case of infinitesimal strain, the Mohr circle is centered near the unit stretch ($S = 1.0$) position on the reference axis, illustrated schematically in Fig. 4(a). A many-fold enlargement of this circle is shown in Fig. 4(b). Stretch, S, and extension, ε, are related as $S = 1+\varepsilon$, so the vertical axis represents extension measured as $+\varepsilon$ and $-\varepsilon$ relative to a new origin at $S = 1.0$. Rotation angles are still measured about the $S = 0$ origin. Angles measured in radians around a curve are defined in terms of arc-length per unit radius, and very small arcs approach straight lines, thus radian values plot approximately along the horizontal axis through the new origin at $\varepsilon = 0$. The old polar reference frame can be approximated, therefore, by a Cartesian system with ε as ordinate and α as abscissa (Fig. 4b).

The directions of maximum and minimum extension

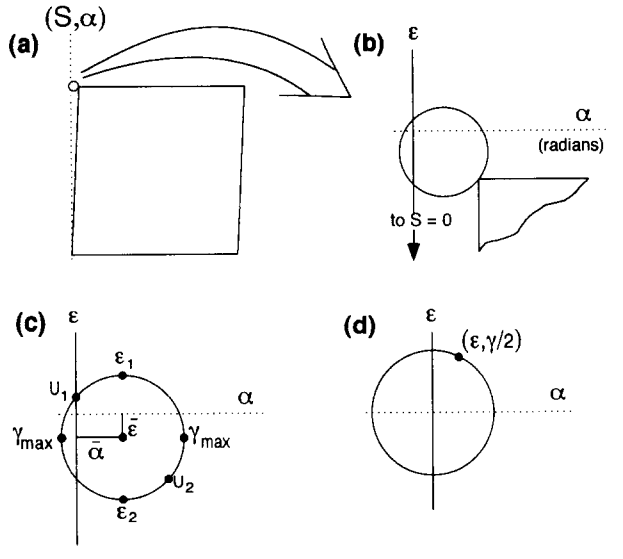

Fig. 4. Relationship between finite and infinitesimal Mohr constructions. (a) For very small strains, finite Mohr circle (in S–α reference frame) is infinitesimal (exaggerated here for clarity). Arrow depicts magnification of view of top left corner of slightly deformed unit square. (b) Dotted line is a new α reference line at distance of one unit up from old (S=0) origin. In new reference frame, co-ordinates are extension ε and rotation in radians, α. (c) Positions of ε_1, ε_2, γ_{max} (see text). U_1, U_2 represents axes of the displacement ellipse (see Fig. 5). (d) Mohr circle centered on origin. There is no infinitesimal rotation or dilatation; co-ordinates of any point on its perimeter are ε and $\gamma/2$ ($= \alpha/2$). The latter is justified because small angles measured in radians approximate their tangents.

ε_1 and ε_2, plot on the infinitesimal Mohr circle's vertical diameter (see Fig. 4c). They share the same angle of rotation $\bar{\alpha}$, so they are therefore directions of no infinitesimal shear strain. All other pairs of orthogonal directions plot diametrically opposite on the Mohr circle and the difference between their α co-ordinates represents their angular shear ψ and, because small angles approximate to their tangents, the angular difference equals the infinitesimal shear strain, γ. Horizontally opposite points on the circle represent directions of maximum shear strain, which are also directions of mean extension $\bar{\varepsilon}$. When the Mohr circle is centered on the origin, there is no infinitesimal rotation or dilatation; co-ordinates of any point on its perimeter are then the components of longitudinal strain and 'engineer's shear strain', ε and $\gamma/2$ (Fig. 4d).

The points U_1 and U_2 farthest from and nearest to the origin on the Mohr circle for infinitesimal strain represent the axes of an ellipse termed the displacement ellipse (Fig. 5) (De Paor 1983). The displacement ellipse is comparable to the strain ellipse in that it represents a general tensor quantity (the displacement gradients tensor), but it is also comparable to the stress ellipse in that its principal axes need not be of the same sign. One axis may represent an outward directed displacement and the other an inward directed displacement, as in the case where the Mohr circle encloses the origin.

The displacement ellipse is an important concept in progressive deformation studies. For non-coaxial deformations, the directions of maximum and minimum displacement are not parallel to the directions of maximum and minimum extension. For example, maximum displacement parallels the boundary of a simple shear zone, but maximum extension is at 45° to the boundary. Furthermore, the directions of maximum displacement and maximum incremental shear strain are both oblique to the boundary of a general shear zone.

Velocity gradients and flow

The term flow is widely used in continuum mechanics to denote the process of permanent, non-elastic, or time-dependent strain. Flow is thus the instantaneous rate of infinitesimal strain. Flow regimes are coaxial if successive increments of infinitesimal strain are parallel and steady if they are also of equal magnitude. Time derivatives of ε and α in the Mohr circle construction for infinitesimal strain plot as strain rates, $\dot{\varepsilon}$, along the

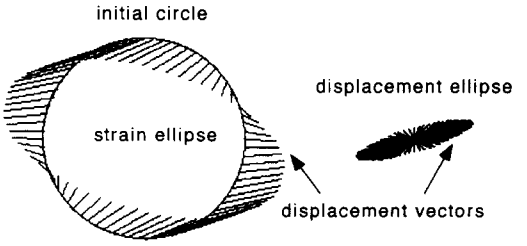

Fig. 5. The displacement ellipse on right is the locus of all displacement vectors joining points on the initial unit circle to the corresponding points on the strain ellipse on left. Note that some displacement vectors point outwards and others inwards.

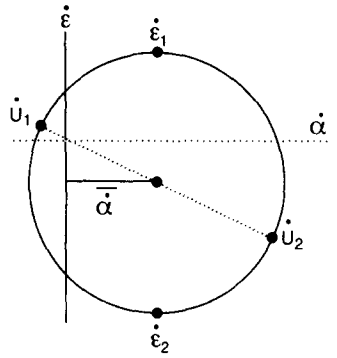

Fig. 6. The flow Mohr circle. $\dot{\varepsilon}_1$, $\dot{\varepsilon}_2$ are directions of maximum and minimum extension rate and share the same angular velocity $\overline{\dot{\alpha}}$. $\dot{U}_1$ and $\dot{U}_2$ are displacement rate axes.

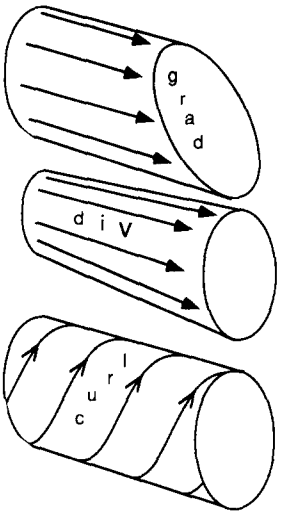

Fig. 7. Schematic representation of gradient, divergence and curl.

vertical axis and angular volocities, $\dot{\alpha}$, along the horizontal axis (Fig 6). Division by time modifies the reference frame without affecting geometrical relations in Mohr space; the Mohr circle now represents flow velocity gradients at an instant in the deformation history.

The flow ellipse is the time derivative of the displacement ellipse. It is important conceptually because it highlights the fact that there is no unique flow plane in general shear. In progressive simple shear, the flow Mohr circle passes through the origin ($\dot{\varepsilon} = 0$). The flow ellipse's short axis is of zero length, and its shape degenerates to a line representing the flow direction. The flow Mohr circle shows that simple shearing is not just a vectorial process, but rather is a tensor phenomenon.

The directions of maximum and minimum extension rate, $\dot{\varepsilon}_1$ and $\dot{\varepsilon}_2$, plot on the flow Mohr circle's vertical diameter (Fig. 6). They share the same angular velocity $\overline{\dot{\alpha}}$, so they maintain orthogonality in the current increment of deformation and are therefore directions of no shear strain rate. Although material in these directions does not shear, it does rotate at the mean rate of $\overline{\dot{\alpha}}$. For steady flow conditions, the $\dot{\varepsilon}_1$ and $\dot{\varepsilon}_2$ directions are fixed in space as material sweeps through them.

Stretching, shearing, divergence and curl

A ductile flow regime possesses three important attributes: gradients, divergence and curl (Schey 1973), represented schematically in Fig. 7. Velocity gradients (*grad*) lead to stretching of the distances between particles, rotation of lines that join them, and shearing of poles to planes. Divergence (*div*) denotes the tendency for isotropic expansion or contraction of material about a point in the flowing mass (see Talbot & Jackson 1987). The vertical offset of the center of the flow Mohr circle, the mean longitudinal strain rate $\overline{\dot{\varepsilon}}$, represents the divergence, which may be centrifugal or centripetal. The Laplacian is a measure of the gradient in the magnitude of the divergence in a flowing mass. Divergent flow and Laplacians are relevant to the understanding of high strain zones with non-parallel boundaries such as spreading thrust nappes.

Vorticity is a description of the way material rotates while it is deforming. Vorticity is recorded by the horizontal offset of the center of the flow Mohr circle, $\overline{\dot{\alpha}}$. It is an unfortunate fact of history that vorticity in classical mechanics is defined in terms of a mathematical function called the *curl* of the velocity field, and is twice the physically meaningful quantity, $\overline{\dot{\alpha}}$. We here define $\overline{\dot{\alpha}}$ as the geologist's vorticity. Engineer's vorticity, defined as the velocity field's curl, is thus twice geologist's vorticity, $2\overline{\dot{\alpha}}$. This is inversely analogous to the case of geologist's shear strain γ vs engineer's shear strain $\gamma/2$. Vortical flow is applicable, for example, to deforming and rotating clasts within a matrix of less vortical flow regime.

MEASUREMENT OF VORTICITY

To evaluate vorticity in rocks, one may choose from three potential reference frames: the finite strain axes (Elliott 1972); the infinitesimal strain axes (Lister & Williams 1983); or the shear zone boundary (this work). Infinitesimal axes are usually chosen in theoretical work (e.g. Lister & Williams 1983), based on the argument that fabrics are sensitive to the instantaneous directions of maximum extension. However, in practice the geologist often has to measure vorticity relative to the only available visible markers, namely, the shear zone boundary and its normal for an external reference frame, and the foliation plus the normal to foliation for an internal reference frame. Provided the reference frame itself is not rotating—a phenomenon called spin (Truesdell 1954, Lister & Williams 1983), it does not matter which is chosen; Fig. 6 shows that the mean rate of rotation of all pairs of perpendicular lines is the same. However, if the shear zone's wall rock is deforming, then only that portion of the vorticity which is internal to the system is measured. The internal vorticity of a flowing mass is strictly defined as the rate at which material sweeps through the infinitesimal extension axes ε_1, ε_2. We may not know whether a particular fabric tracks the finite or infinitesimal principal directions so internal vorticity may be difficult to quantify. However,

the sense of rotation is all that is measured in practice and so the choice of foliation as an *ad hoc* internal reference frame should not present a problem.

Kinematic vorticity number

Internal vorticity is positive or forward directed when material sweeps through the reference axes in the direction in which they are themselves rotating, otherwise it is negative or backward. For positive cases, it is useful to further classify vortical flow regimes in two dimensions by the amount of vorticity relative to the amount of longitudinal strain. The commonest measure of this ratio is the kinematic vorticity number W_n (Truesdell 1954), which can be defined in several ways; most simply, it is the cosine of the angle ν between the eigenvectors (Bobyarchick 1986) (Fig. 8),

$$W_n = \cos(\nu). \quad (1)$$

In the case of progressive simple shear, $W_n = \cos 0 = 1.0$. This is consistent with the fact that the flow Mohr circle touches the reference axis at one point only. In the case of sub-simple shear, W_n has a value between 0.0 and 1.0; correspondingly there are two non-orthogonal eigenvectors of the flow Mohr circle.

According to Means *et al.* (1980), petrofabric development may be controlled by the kinematic vorticity number of the flow immediately prior to the fossilization of the fabric. This relationship has been demonstrated to hold for calcite lattice preferred orientations (Wenk *et al.* 1987), but quartz fabrics appear to be more complexly related to W_n (Schmid & Casey 1986).

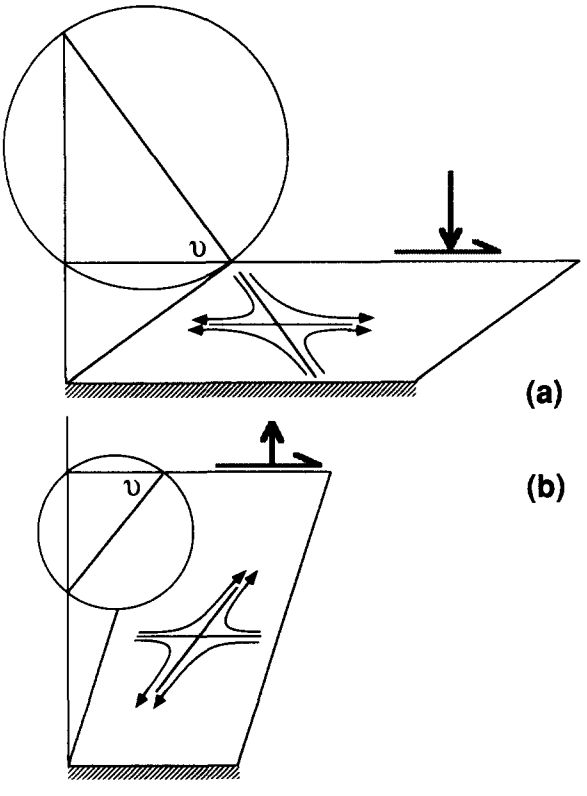

Fig. 8. Mohr and geographical space representations of kinematic vorticity number $W_n = \cos \nu$, where ν is angle between eigenvectors (after Bobyarchick 1986). Dextral sub-simple shear zone in (a) is narrowing and in (b) is broadening.

Acceleration

In rigid-body mechanics, it is not sufficient to describe the position and velocity of a particle; for a full description its acceleration is also required. Similarly, finite strain and flow are only a partial description of a rock's deformation; acceleration completes the story. In kinematic studies it is usual to assume, for the sake of simplicity, that the flow regime remains constant with time, but this is unlikely to be true in general. Changes are inevitable at the start and end of a tectonic event and where the boundaries of a high strain zone are curved. Acceleration is critically important in kinematic studies because the consequent change in strain rates may alter the operative deformation mechanisms. Microstructures attributed to a change in *P–T* environment may be due instead to acceleration or deceleration of deformation. Furthermore, we do not know whether it is the maximum displacement rate (long axis of the flow ellipse), maximum extension rate (vertical coordinate on the flow Mohr circle), maximum shear strain rate (diameter of the flow Mohr circle) or other quantity (e.g. mean displacement rate) that controls the choice of deformation mechanisms.

If velocity gradients change with time, the flow becomes unsteady or accelerating and the flow Mohr circle's size and position is a function of time. An accelerating deformation is represented by an acceleration Mohr circle in $\ddot{\varepsilon}/\ddot{\alpha}$ space (Fig. 9a). Change in the divergence of the flow is recorded by the vertical offset of the acceleration Mohr circle along the $\ddot{\varepsilon}$ axis. This means that the rate of dilatation, or rate of inflation, is speeding up or slowing down. A horizontal shift of the Mohr circle's center represents a spinning deformation in which the principal stretching directions change with time. The rate of spinning is given by the difference between internal vorticity and total vorticity $\ddot{\bar{\alpha}}$, per unit time.

Acceleration and rotation reversals

For steady sub-simple flow regimes, the eigenvectors of finite strain and flow are parallel. These eigenvectors are not merely directions of no net rotation, rather they are directions which have never rotated throughout deformation. This distinction is important for fabric considerations. In nature, it is likely that either one or both of the components of a sub-simple shear will grow or decay with time. For example, a constant progressive simple shear in an overthrust orientation may be accompanied by a gradual build-up of vertical pure shear due to the advance of an overlying thrust sheet, or by the decay of pure shear due to erosional removal of overburden. Alternatively, overburden may generate a growing coaxial spreading flow in a thrust sheet during the commencement of ramping and accompanying shear deformation. The waning stages of a deformation event

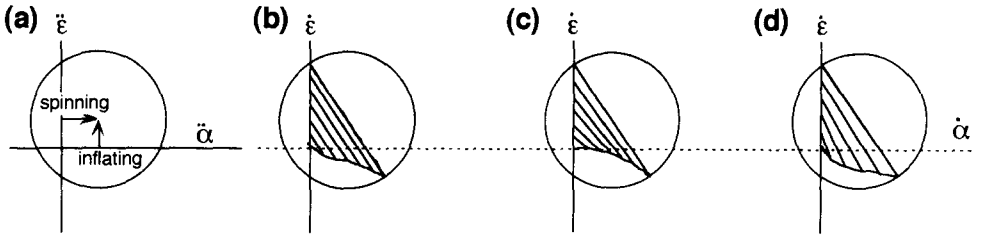

Fig. 9. Representation of acceleration using Mohr circles. (a) Vertical offset of circle on $\ddot{\varepsilon}/\ddot{\alpha}$ axes represents an inflating deformation in which there is a change in divergence. Horizontal offset represents a spinning deformation in which there is a change in the principal flow directions. (b)–(d) Flow Mohr circles for the same cumulative deformation but with different flow histories. Only the reference diameters of early Mohr circles are drawn for the sake of clarity. (b) Constant flow regime in which eigenvectors, and thus reference diameters, remain parallel. (c) Coaxial component of flow builds up faster than the vortical component. (d) Vortical component builds up faster than non-coaxial flow component.

may also involve different rates of decline in the pure and simple components of progressive general shear. The consequences of accelerating flow regimes are illustrated using the series of Mohr circles in Figs. 9(b)–(d). There are three degrees of freedom which can be represented by the changes in center and radius of the circle. For the sake of clarity, only one 'reference' diameter of smaller Mohr circles is shown. The full circle is shown for the last state recorded.

Figure 9(b) illustrates the case of a constant flow regime. Because the eigenvectors must remain constant in orientation, successive reference diameters of the Mohr circles are parallel. In Fig. 9(c) the build-up of the coaxial component of flow exceeds that of the non-coaxial component. Successive reference diameters are more steeply inclined, implying a larger angle between the eigenvectors. In contrast, Fig. 9(d) shows the gradual decrease in this angle resulting from a greater build-up of non-coaxial flow. The final state is identical in each case. Note that all directions oriented between the first increment and final cumulative reference diameters have undergone a transient reversal in the signs of their angular velocities. The result is recovery of initial orientations followed by further rotation. Lines oriented between the final cumulative and final incremental reference diameter have reversed their sense of rotation, but have not yet recovered their initial orientations (Fig. 10). This situation is reminiscent of the shear of lines as a function of orientation (Fig. 3), and the lengthening of lines that initially shorten.

PRACTICAL ANALYSIS OF GENERAL SHEAR

In order to determine the complete deformation history of a rock, the relative contributions of pure shear, simple shear, rigid rotation and dilatation during each increment of time must be evaluated. This information is essential for meaningful pressure–temperature–time–deformation paths. Finite strain markers record the geometry of the final state only. Kinematic analysis is the search for indicators of the flow regime operative during deformation. Of particular interest are fabrics that reveal the sense of vorticity of the flow. In special circumstances, it may be possible to evaluate the kinematic vorticity number.

One of the oldest concepts of structural geology is the symmetry principle of Curie (1894). It implies that symmetric fabric patterns result from coaxial progressive deformation of a random protolith fabric, whereas asymmetry may be expected to result from a vortical deformation path. The association between fabric symmetry and deformation path is not, however, that simple (Choukroune *et al.* 1987). It is important to distinguish between passive and active strain markers, between finite and infinitesimal markers, and between material and non-material lines.

Foliation as a strain marker

The simplest method for the determination of strain in a shear zone assumes that (i) the cross-sectional trace of

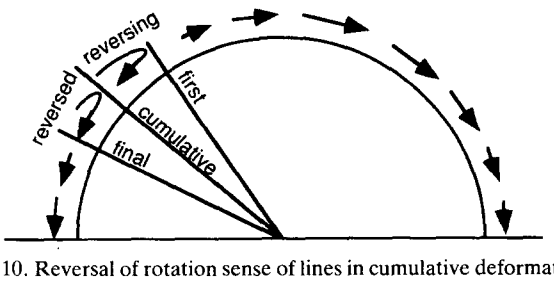

Fig. 10. Reversal of rotation sense of lines in cumulative deformation. Arrows indicate the direction of rotation. See text for discussion.

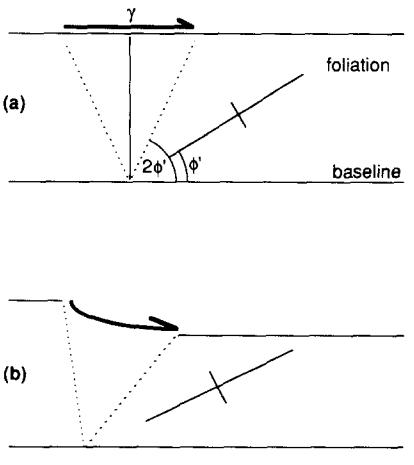

Fig. 11. Relationship between foliation direction ϕ' and shear strain γ in (a) simple shear zone, (b) zone of sub-simple shear. Dashed lines are traces of circular sections of the strain ellipsoid.

foliation represents the long axis of the strain ellipse ϕ' and (ii) the strain is ideal simple shear (Fig. 11a). The equations for simple shear are:

$$\gamma = 2/\tan 2\phi' \quad \text{(Ramsay \& Graham 1970)} \quad (2)$$

$$S_1 = \cot \phi' \quad (3)$$

$$S_2 = \tan \phi' \quad (4)$$

and

$$\gamma = 2 \sinh E, \quad (5)$$

where

$$E = (1/2) \ln (S_1/S_2) \quad \text{(Nadai 1963)}. \quad (6)$$

Because the angle ϕ' between the foliation and shear zone boundary is measured in the rock, these calculations can be carried out rapidly on field location. The main drawback is the assumption of ideal simple shear. If the deformation is a sub-simple shear as indicated in Fig. 11(b), the method is invalid and angle ϕ' may become very small at quite low strain intensities.

Asymmetry of SNFLS and SNILS

One way to determine the relative contributions of pure and simple shear during steady flow is to find the surfaces of no finite longitudinal strain (SNFLS) and compare these with known surfaces of no incremental longitudinal strain (SNILS; de Sitter 1956, Flinn 1962, Ramsay 1967, Talbot 1970, Passchier 1988). Ramsay (1967) showed that in progressive pure shear, the SNFLS and SNILS are coaxial. Lines that progressively shorten (folds), lines that originally shorten and then lengthen (boundinaged folds), and lines that progressively lengthen (boudinage), are developed symmetrically about the principal axes. For progressive simple shear and sub-simple shear, SNFLS and SNILS are oblique to each other so that there are two asymmetrically developed zones of boudinaged folds; the orientation distribution of these can be measured in the field and can distinguish between a predominantly pure-shearing or a simple-shearing history. The relative size of the asymmetrical zones may even permit an estimate of the relative contributions of the two. For progressive super-simple shear, there is a zone of lines that lengthen first and then shorten, resulting for example in the folding of previously boudinaged veins.

Orientation of eigenvectors

In Fig. 12(a), polar co-ordinates $(\xi_1, 0)$ and $(\xi_2, 0)$ on the Mohr circle represent the two non-rotating lines (eigenvectors) in the rock and the eigenvalues ξ_1 and ξ_2 are the principal values of the irrotational strain component. T is the transverse component of deformation. The angle 2ν, measured around the arc between ξ_1 and ξ_2 in Mohr space, provides the angle ν between these two eigenvectors in real space, where

$$\tan (\nu) = (\xi_1 - \xi_2)/T. \quad (7)$$

The orientation of one eigenvector is fixed to the flow plane of the simple shear component, but the other eigenvector has an orientation that is dependent on the pure shear and simple shear contributions to sub-simple shear. The smaller the irrotational component, the smaller is the angle between ξ_1 and ξ_2. The important conclusion is that determination of the eigenvectors in a general shear zone may lead to information about the relative contributions of irrotational vs rotational strain. Much recent effort has centered on ways of identifying the eigenvectors (Ramberg 1975, Ghosh & Ramberg 1976, Passchier 1987).

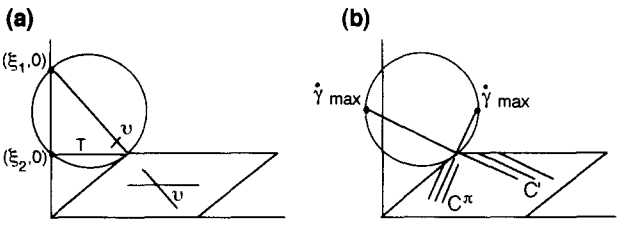

Fig. 12. (a) Relationship between the eigenvectors of sub-simple shear in Mohr space and geographical space. Equation (7) follows from this geometry. (b) Proposed relation between synthetic (C') and antithetic (C^{π}) shear band orientations and directions of maximum shear strain rate $\dot{\gamma}$.

Shear bands

Shear bands have been used by a number of workers to obtain sense of shear (e.g. Weijermars & Rondeel 1984, Bobyarchick 1986, Dennis & Secor 1987). Bobyarchick (1986) suggested that the inclined eigenvector ξ_2 may represent the orientation of shear bands in natural shear zones. If correct, then the measured angle between shear bands and the overall flow plane could be used to estimate the relative contributions of pure and simple shear in natural examples. However, the eigenvector directions are not directions of maximum shear strain (in fact, they may undergo quite low angular shears) and the inclined eigenvector is an unstable direction where there is extension parallel to the shear zone boundary and shortening perpendicular to it. If a plane is deflected slightly from this direction, it will continue to rotate away progressively.

Conjugate shear bands (extensional crenulation cleavage) in zones of non-coaxial strain have been documented by several workers. Platt & Vissers (1980) suggested that conjugate sets might indicate a coaxial flow regime, but subsequently Platt (1984) showed that conjugate sets could occur if there was deviation from progressive simple shear. Harris & Cobbold (1985) showed the development of conjugate shear bands during bulk simple shearing if sliding was permitted along pre-existing foliation planes. Behrmann (1987) reported the occurrence of conjugate sets of shear bands in a mylonite from the base of a known thrust nappe. The mylonite gave a consistent shear sense using quartz petrofabric data, and was thought to be developed in a non-coaxial (sub-simple shear) regime. One shear band

set was inclined at 30° towards the flow direction and sheared synthetically; the other was inclined at 60° upstream and sheared antithetically. These angles suggest a possible association with the directions of maximum shear strain rate (Fig. 12b) and not with the eigenvector directions.

In view of the alternative interpretations, shear band orientations are, at best, semi-quantitative indicators of the shear components. If shear bands approximately bisect the angle between the eigenvectors in zones of relatively low strain, then they will become progressively rotated into alignment with the flow plane at higher strains.

Rotation of rigid spherical objects

Rigid quasi-spherical objects such as garnet crystals or pyrite framboids are excellent kinematic indicators (Rosenfeld 1968, Schoneveld 1977), but the relationship between internal and external fabrics may be complex. From the traditional interpretation of snowball garnets (e.g. Schoneveld 1977), the porphyroblast overgrows the existing foliation as the garnet rotates. The internal fabric is dragged around as the garnet rotates faster than the foliation. In progressive simple shear the rigid rotation rate for rigid objects is half the instantaneous shear strain rate (Fig. 13):

$$\dot{\omega} = \frac{\dot{\gamma}}{2}. \tag{8}$$

This is because half of the angular shear experienced by the pole to the shear zone is a result of rigid rotation and the other half is caused by the pure shear at 45° to the shear zone boundary. In progressive pure shear, the matrix flows symmetrically around rigid obstructions and applies equal fiber loading stress to each side, so the object does not rotate. Applying the same arguments to general shear, rigid spheres such as garnets are unaffected by the pure shear component of deformation and rotate only in response to the rigid rotation component (Ghosh & Ramberg 1976).

At low finite strains, foliation lags behind a spherical

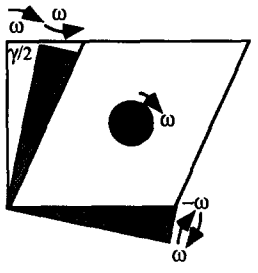

Fig. 13. Simple shear may be factored into a component of rigid rotation through angle ω whose tangent is half the shear strain, and a pure shear component oblique to reference axes. The latter component adds to the rotation of shear zone's pole but cancels the zone boundary's rotation. A circular rigid object responds to rigid rotation ω but not to the irrotational component of deformation. Note that this argument may be applied to every increment of deformation and thus holds even where actual deformation path is not that represented by arrows.

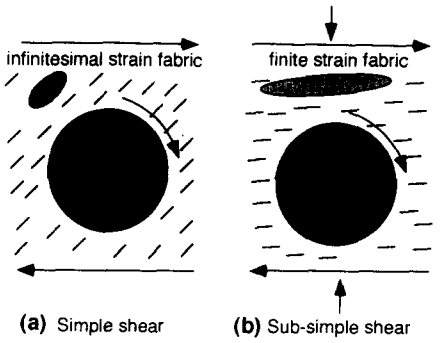

Fig. 14. Illustration of possible ambiguities arising from spiral inclusion trails in rigid porphyroclasts such as garnets. (a) Conventional trails result from garnet rotating more rapidly than foliation. (b) Relatively rapid rotation of foliation during sub-simple shear may be wrongly interpreted.

rigid porphyroblast in simple shear (Fig. 14a). This is self-evident for a steady state foliation, which by definition does not rotate. Where the foliation tracks the finite strain axes, it's rotation rate decelerates as it approaches parallelism with the shear zone boundary and so the total rotation of the rigid grain must exceed that of the foliation. If the shear zone undergoes sub-simple shear and broadens with time, then the foliation remains at a high angle to the zone boundary and enhances the rotational pattern of inclusions. However, if there is a component of pure shear acting to narrow the shear zone and the foliation tracks the finite strain axes, then the foliation may rotate faster than the rigid object provided the latter does not rotate more than 90°. In a domain of super-simple shear that includes a rigid object, a foliation which tracks the finite strain direction may rotate faster than the object at all times, resulting in a false interpretation of the sense of shear even at high strain. Interpretation of snowball garnets thus relies heavily on the correct interpretation of the relationship between internal and external fabrics.

Curvature of fibers around rigid inclusions can be used to obtain the rotational component of strain provided there is a clear distinction between face-controlled fibers and those that track the incremental stretch direction (Ramsay 1980, Ramsay & Huber 1987). A difficulty arises, however, if the fibers do not form parallel to the incremental stretch direction (Urai *et al.* 1991).

Rotation of rigid elongate objects

Reverse rotations of objects are generally possible in homogeneous flow regimes only if the deformation is sub-simple shear, the objects are relatively rigid, and they are more elongate than a critical value. As shown by Gay (1968) and Ghosh & Ramberg (1976), there is a simple relationship between the rotation angle of rigid spherical objects and that of elongate objects in general shear zones with constant flow parameters, i.e. where the eigenvectors remain constant throughout. The more elongate objects are more susceptible to the pure shear component and tend to rotate both forwards and backwards. By measuring the angle of rotation of rigid

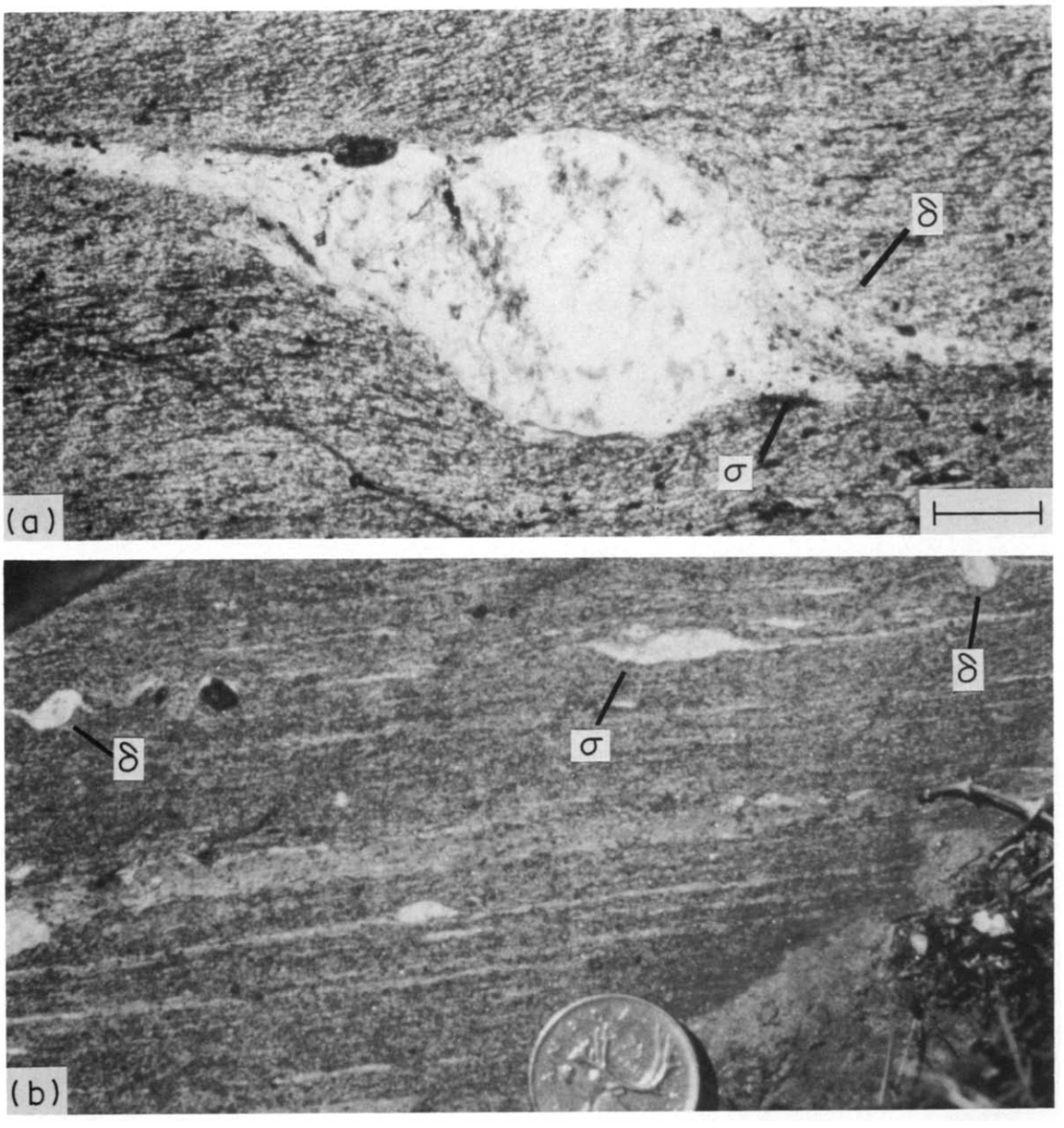

Fig. 15. (a) Complex σ–δ feldspar grain from mylonitic granodiorite, Pinaleño Mountains, Arizona. Both σ and δ tails step up to left and become parallel to foliation, consistent with sinistral shear sense. Plane light. Scale bar is 250 μm. (b) Outcrop photograph of σ and δ feldspar grains on same flow plane in amphibolite gneiss, Parry Sound, Ontario. Tails on all porphyroclast systems step up to left and become parallel to foliation, consistent with sinistral shear sense. Coin diameter is 2.4 cm. See text for discussion.

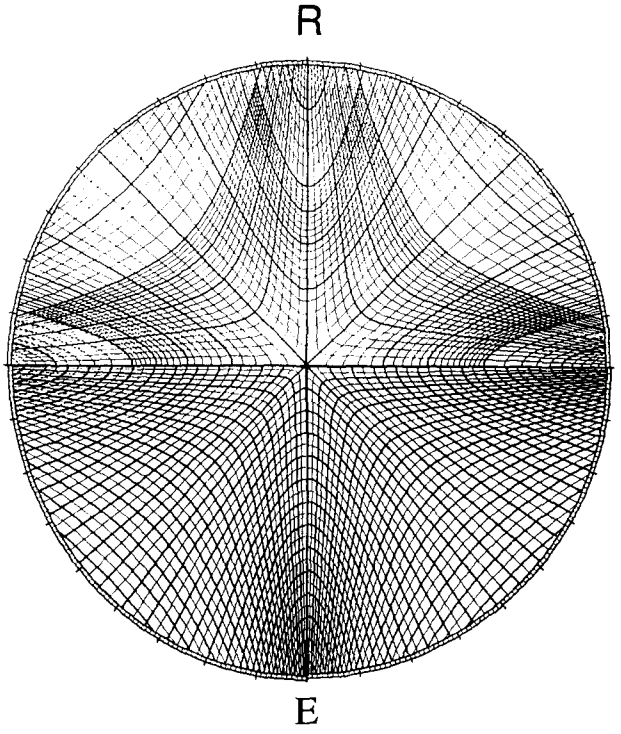

Fig. 16. The hyperbolic net (see De Paor 1988 for a larger version). R is axial ratio, shape factor $E = (1/2) \ln (R)$.

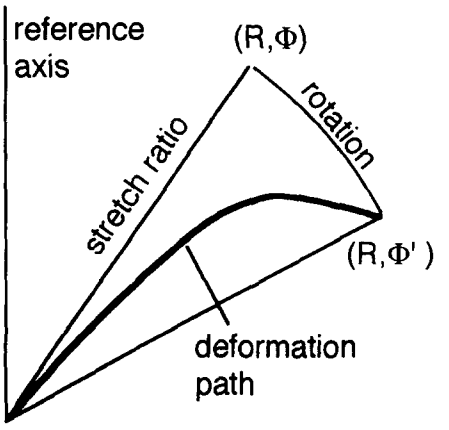

Fig. 17. Plot of non-coaxial deformation path on the hyperbolic net. Stretch and rotation factors are represented by pie segment.

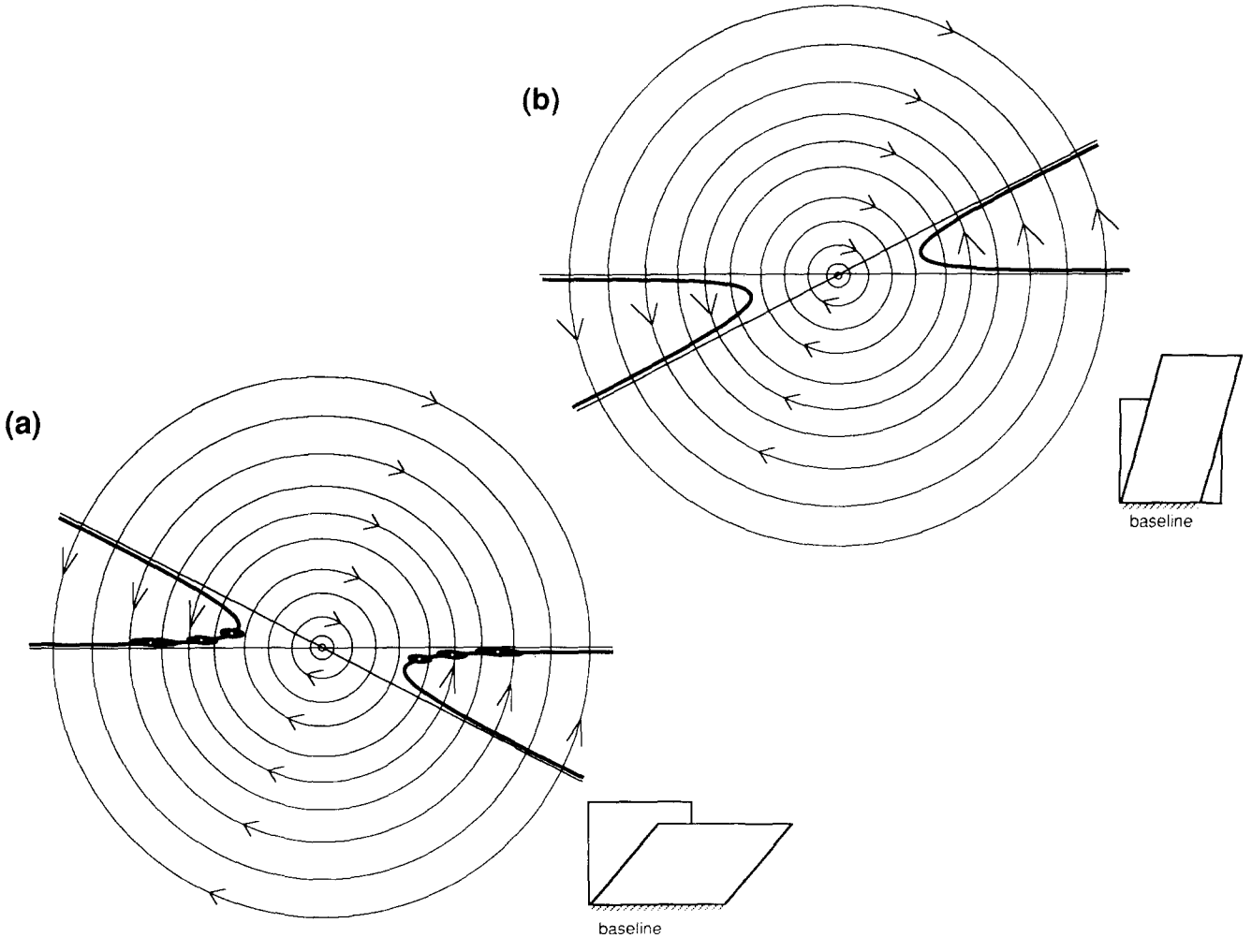

Fig. 18. Behavior of rigid objects plotted on the hyperbolic net. Thin straight lines are eigenvectors. Thin curved lines represent trajectories, arrows indicate direction of rotation. Note back rotation on concave side of hyperbola (heavy line). Stable end orientations marked by representative ellipse shapes. (a) Narrowing sub-simple shear, (b) Broadening sub-simple shear. Squares represent undeformed states, and parallelograms deformed states.

objects of known axial ratio, such as garnets that contain inclusions, with respect to the foliation around them it may be possible to estimate W_n. This technique was successfully applied by Vissers (1989) to obtain W_n and the total strain from the rotation of pre-mylonitic garnets in a schist (see also Vissers 1987).

σ and δ grains

Porphyroclasts with recrystallized tails are extremely useful for sense of shear determination in high strain zones (see Simpson & Schmid 1983, Lister & Snoke 1984, Passchier & Simpson 1986). The sense of shear is given by the sense of 'stair-stepping' of the tails on either side of the porphyroclast. Tails that step up to the right give a dextral shear sense. Grains with wedge-shaped tails are σ grains. Grains with very narrow tails that cross the reference plane are δ grains. The distinction is more than pedantic.

Passchier & Simpson (1986) showed that the presence of σ or δ tails depends on the rate of recrystallization $\dot{R}$ to shear strain rate $\dot{\gamma}$. If $\dot{R}/\dot{\gamma}$ is high, the flow of recrystallized material in the tails away from the porphyroclast is continually supplemented by the production of new recrystallized grains, resulting in the wedge-shaped tails of σ grains. If $\dot{R}/\dot{\gamma}$ is low, there is insufficient new recrystallized material added to the tail to form a wedge and the narrow tail that results becomes dragged around with the rotating δ-type host grain. The δ grains are usually only found in high strain, ultramylonite zones.

Passchier (1988) suggested that the degree of 'stair-stepping' of wedge-shaped recrystallized tails on σ-type porphyroclasts can be used to determine W_n. The method is based on the assumption that σ grains and mylonite foliations give the instantaneous stretching direction and the eigenvector for flow, respectively, regardless of the directions of the diplacement axes.

Complex σ–δ grains

Some porphyroclast systems have more than one set of tails (e.g. Fig. 15a, and see Davidson *et al.* 1982, Hanmer 1984). Passchier & Simpson (1986) reproduced these by starting with a δ grain (low $\dot{R}/\dot{\gamma}$) and then varying the $\dot{R}/\dot{\gamma}$ parameters so that $\dot{R}$ increased with respect to $\dot{\gamma}$. Natural examples imply that: (a) the temperature rose during a constant strain rate deformation; (b) the shear zone remained at the same temperature during a decreasing strain rate deformation; or (c) the shear zone maintained a constant temperature and strain rate, but the grain itself was initially elliptical in cross-section, and therefore changed its rotation rate during deformation.

The existence of σ, δ and complex porphyroclast systems (Passchier & Simpson 1986) in the same outcrop is not uncommon (e.g. Fig. 15b). Such occurrences preclude Bell & Johnson's (1992) explanation of δ grain tail geometry as the result of three separate, mutually perpendicular orogenies. If all grains were identical in mineralogy and were spherical to start with, then σ grains would indicate a high $\dot{R}/\dot{\gamma}$, and δ grains would indicate a low $\dot{R}/\dot{\gamma}$ (Passchier & Simpson 1986). However, if the two types of grains are of the same mineral and in the same rock then they cannot reflect great differences in the tempeature-controlled recrystallization rate. If they are on the same flow plane, or nearly so, as in Fig. 15(b), then a large gradient in strain rate is also unlikely. One way to form grain associations like the one in Fig. 15(b) is to start with grains of very different axial ratio and/or orientation.

Analysis of strain and strain path using the hyperbolic net

Building on the pioneering work of Ramberg (1975) and Ghosh & Ramberg (1976), we now demonstrate that the concepts of finite general shear and porphyroclast morphology provide a framework in which a great variety of strain markers and kinematic indicators may be understood. Porphyroclasts are indicators of both strain and flow, and the hyperbolic net of De Paor (1988) can be used to analyze the vorticity and strain path as well as the finite strain state.

De Paor (1988) described the use of the hyperbolic net for the implementation of the R_f/ϕ technique of Ramsay (1967), Dunnet (1969) and Dunnet & Siddans (1971), the shape factor grid of Elliott (1970), and the θ-curve method of Lisle (1977, 1985). Strained objects are assumed to be perfectly passive ellipses in all of these words. The hyperbolic net is a polar graph of ellipse shape versus orientation (Fig. 16). Orientation ϕ is measured around the periphery of the net and ellipse shape is plotted radially outward from the origin. Diametrically opposite points on this plot represent the same ellipse but there are two scales for describing ellipse shape: axial ratio R and shape factor $E = 1/2 \ln (R)$ (see De Paor 1988 for details). Note that a circle (axial ratio = 1, shape factor = 0) plots at the origin. Two sets of hyperbolae adorn the hyperbolic net. Those with vertical and horizontal asymptotes and diagonal vertices are trajectories that trace the paths of ellipses undergoing strain in the direction of the net axis. Hyperbolae with vertical and horizontal vertices and non-orthogonal asymptotes are loci of equal incremental strain and serve to determine the 50%-of-data curve (Dunnet 1969), also known as the $\theta = 45°$ curve (Lisle 1977, 1985).

The hyperbolic net is used with a tracing overlay in a manner analogous to a steronet. To represent a strain path, the cumulative finite strain ellipse is plotted for successive points in time. A coaxial deformation involves no change in strain ellipse orientation and so is recorded by a straight path directed radially out from the origin. Increments of rigid rotation change the orientation but not the shape of the strain ellipse and so plot on a circular arc. Shear in general follows a curved path (Fig. 17) from the initial point $(1, \phi)$ to the point representing the final state (R, ϕ'). The effects of an increment of deformation upon a pre-existing ellipse may be modelled by applying small increments of irrotational stretch and rigid rotation. The ellipse is moved

along a hyperbolic trajectory to simulate stretch and the tracing overlay is rotated to simulate rigid rotation.

Analysis of vorticity using the hyperbolic net

The hyperbolic net can also be used to determine another hyperbolic locus called the 'stable-end' curve which gives a simple method for obtaining W_n from rigid elliptical porphyroclasts in mylonites. The basis for this method is the theoretical work of Jeffrey (1923), Ghosh & Ramberg (1976), Freeman (1985) and Passchier (1987) concerning the motion of ellipsoidal, perfectly rigid particles in steady non-coaxial flow. Elongate objects inclined downstream in a shear zone tend to rotate backward if there is positive extension along the shear zone boundary, i.e. the shear zone is narrowing (Fig. 18a), and elongate objects inclined upstream tend to rotate backward if there is a contraction along the boundary, i.e. the shear zone is broadening (Fig. 18b). As illustrated in Fig. 18, lines in all orientations in the acute angle between the eigenvectors rotate backwards, but not all elliptical objects do so. A rigid sphere ($R = 1$) is unaffected by the irrotational component of general shear and responds only to the rotational component. Therefore it will rotate in the direction of shear, albeit more slowly than the shear strain rate (for simple shear it would rotate at half that rate). Because all lines in the acute field rotate backwards and spheres rotate forwards, there must be critically shaped and oriented elliptical objects (R, ϕ) that do not rotate at all, and a minimum axial ratio below which all objects rotate with the flow.

In the Appendix we provide proof that all rigid ellipses which do not rotate plot on a hyperbola asymptotic to the eigenvectors. Half of these are unstable positions from which objects flee given a slight nudge. The other half are the 'stable end' positions (those marked by a dot on Fig. 18) (Ghosh & Ramberg 1976, Freeman 1985, Passchier 1987). The orientation of a stable ellipse is a function of its axial ratio and of the kinematic vorticity number W_n. The minimum axial ratio, R_m, for stable orientation plots at the apex of the hyperbola and is related to W_n by

$$W_n = (R_m - 1/R_m)/(R_m + 1/R_m). \quad (9)$$

The orientation ϕ_m of this individual is also related to flow,

$$W_n = \cos(2\phi_m) \quad (10a)$$

$$= \cos(\nu). \quad (10b)$$

All other stably oriented ellipses plot along one limb of the hyperbola, whose formula is

$$B = W_n/\cos 2\phi, \quad (11)$$

where ϕ is measured relative to ϕ_m and B is an alternative description of ellipticity, related to the axial ratio, R, and Elliott shape factor, E, respectively by,

$$B = (R - 1/R)/(R + 1/R) \quad (12a)$$

and

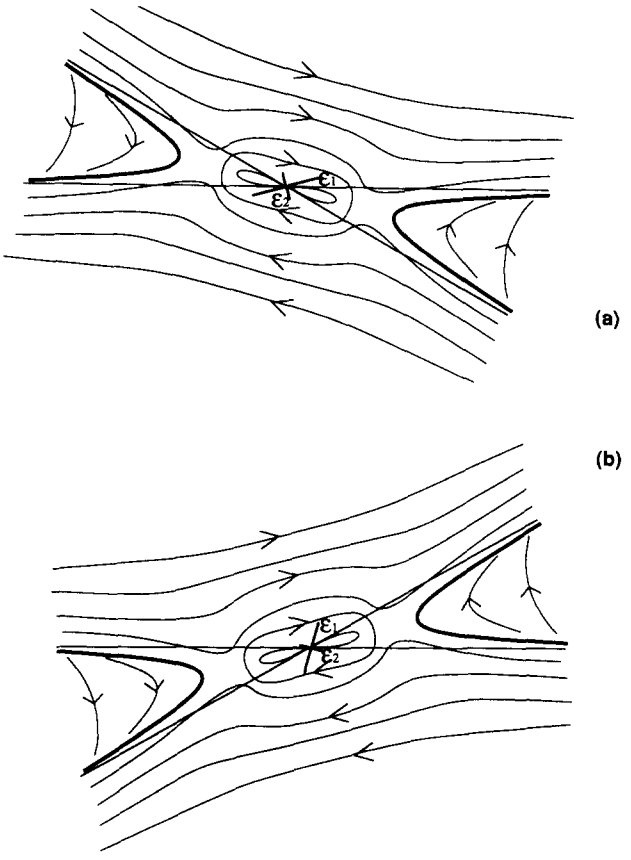

Fig. 19. Behavior of deformable objects in (a) narrowing sub-simple shear, and (b) broadening sub-simple shear, depicted schematically on the hyperbolic net. Details of trajectories (thin curved lines) depend on the ductility of porphyroclasts. ε_1 represents the infinitesimal stretching axis. Other features as in Fig. 18.

$$B = \tanh(2E). \quad (12b)$$

Equation (11) is analogous to equation (A22) of De Paor (1988), therefore the hyperbolic locus of stable end positions is given by fitting a curve from the hyperbolic net asymptotically between the flow eigenvectors.

Rotation of deformable objects

Deformable ellipsoidal objects may possess internal vorticity which differs from that of the bulk flow. During deformation, their long axes and axial ratios change and a succession of new material lines move through the immaterial axes of the ellipsoid. If objects are not perfectly ellipsoidal, the migration of their axes may be quite complex. We can never determine the vorticity of a single object, but nevertheless we can use a set of deformable objects to determine the bulk flow vorticity. The behavior in cross-section of deformable ellipsoidal grains is schematically illustrated in Fig. 19. Following Lisle (1985), we assume that the grain's rotation axis remains perpendicular to the flow direction (cf. Lister & Price 1978). The obvious difference from Fig. 19 is that trajectories are no longer circular arcs. Elliptical cross-sections become greater or smaller in axial ratio depending on the object's orientation relative to the fields of extensional and contractional infinitesmal strain. An object initially plotting on the concave side of the hyper-

bola rotates backward while deforming until it reaches its instantaneous stable end configuration. It then proceeds to deform while rotating and follows a trajectory that coincides with the hyperbola. Eventually, all back-rotated objects become extremely stretched and oriented virtually parallel to the stable eigenvector, i.e. parallel to the foliation. Deformable objects that initially plot on the convex side of the hyperbola display complex trajectories. Most rotate forward, either spinning rapidly and pulsating in axial ratio if they were intially relatively fat, or slowing down and reaching the hyperbola if they were elongate. However, some objects that plot near the hyperbola undergo a period of back-rotation as their axes spin backwards and sweep through material lines.

Practical implementation

Axial ratios R and orientations ϕ of porphyroclasts are measured relative to the shear zone boundary, or relative to foliation in a narrowing shear zone in which shear strain is judged to be so high that foliation and boundary are virtually parallel. Axial ratio and orientation data are plotted on the hyperbolic net, along with shear sense, using symbols to distinguish back- and forward-rotated σ grains, δ and complex δ–σ grains. Just as with steronet data, the points when plotted are quite independent of their location in the rock. The net is rotated like a stereonet and a hyperbola (representing the locus of stable ends) is drawn asymptotic to the shear zone boundary direction so as to enclose the field of back-rotated or σ-type grains and then the hyperbola's other asymptote is drawn. This second asymptote is inferred to be the inclined eigenvector and the cosine of its inclination ν to the flow plane is W_n (equation 1).

Takagi & Ito (1988) and Malaveille & Ritz (1989) have described ellipsoidal porphyroclasts that are inclined downstream and have σ tails attached to their broad sides. They record backward rotation and plot inside the hyperbola between the flow eigenvectors (Fig. 20). Objects such as elongate garnets that record backward motion also plot in this field. δ grains, which indicate continuous forward rotation, occupy the field outside of the hyperbola. Complex σ–δ grains also indicate continuous forward motion, with formation of the σ trails when the rotation of δ grains slows down as they approach the stable end orientation (Fig. 20). The upstream-inclined mica 'fish' of Lister & Snoke (1984) commonly have extremely thin and straight tails, or no tails at all, consistent with a generally low $\dot{R}/\dot{\gamma}$. They may have rotated forward without producing tails until they approached their stable end orientation where rotation rates would be slow enough to allow recrystallization to form long, straight tails. Ellipsoidal σ grains that have tails attached to their narrow ends and that are inclined upstream may have had starting orientations close to their final orientations. In addition, deformable upstream-inclined grains are subject to slight back-rotation in the zone of complexity where the trajectories cross the stable eigenvector (Figs. 19 and 20). Other microstructures that fit this model include myrmekitic feldspars (Simpson & Wintsch 1986), which are expected to be in stable end orientations, and fractured feldspars which can form in a variety of orientations but which are most likely to fracture when their cleavage planes are aligned along directions of maximum shear strain rate (Fig. 20).

One problem with this approach is that there may be little data in the region around the unstable eigenvector because all elongate objects rotate away from this line. Therefore, just as in shear sense determination where correct interpretation depends on the statistical distribution of grains, a large population of grains is needed, the maximum combination of methods to determine W_n should be used, and the foliation should represent a single, progressive deformation. The analysis should include σ and δ or complex δ–σ type porphyroclasts, and there must be relatively equant grains in addition to highly elongate ones as the former give more accurate results. Thin sections should be cut thicker than normal to reveal the orientation of the porphyroclast in the third dimension; individuals that are cut obliquely or that impinge upon their neighbors should be rejected (Passchier 1987). The key to successful application of this technique is the recognition in the rock of objects that: (1) are rigid vs those that are deformable; (2) are in their stable end positions vs 'immature individuals'; and (3) have rotated backward vs those (more common) that have rotated forward.

Narrowing vs broadening shear zones can be distinguished on the basis of their preserved microstructures only if the shear zone boundary orientation is known (Fig. 20). In the case of broadening zones, the stable eigenvector and therefore the foliation, is maintained at a significant angle to the zone boundary which is now the unstable eigenvector.

Flow eddies and fabric disturbance

The existence of stiff or relatively ductile grains in a flowing matrix leads to a complex, locally spinning flow pattern. Figure 21(a) illustrates the streamlines of a flowing mass that includes a stiff grain, itself undergoing super-simple shear, in a relatively ductile matrix undergoing sub-simple shear (the opposite case, Fig. 21b, is of mainly theoretical interest). The pattern is centered on the grain causing the disturbance. The important implication of Fig. 21(a) is the disturbance of the ideal sub-simple shear flow pattern around the boundary of the stiff grain. Drag on the grain's surface, combined with deflection of the flow lines, may lead to a situation in which smaller grains in a satellite position undergo a local rotational couple (Fig. 21a). Rotation may be opposite to that of the main vortex, even where grains are circular or near-circular in cross-section.

Asymmetric boudins and sheath folds

The distribution of asymmetric rigid or deformable boudins and folds may also be controlled by eigenvector

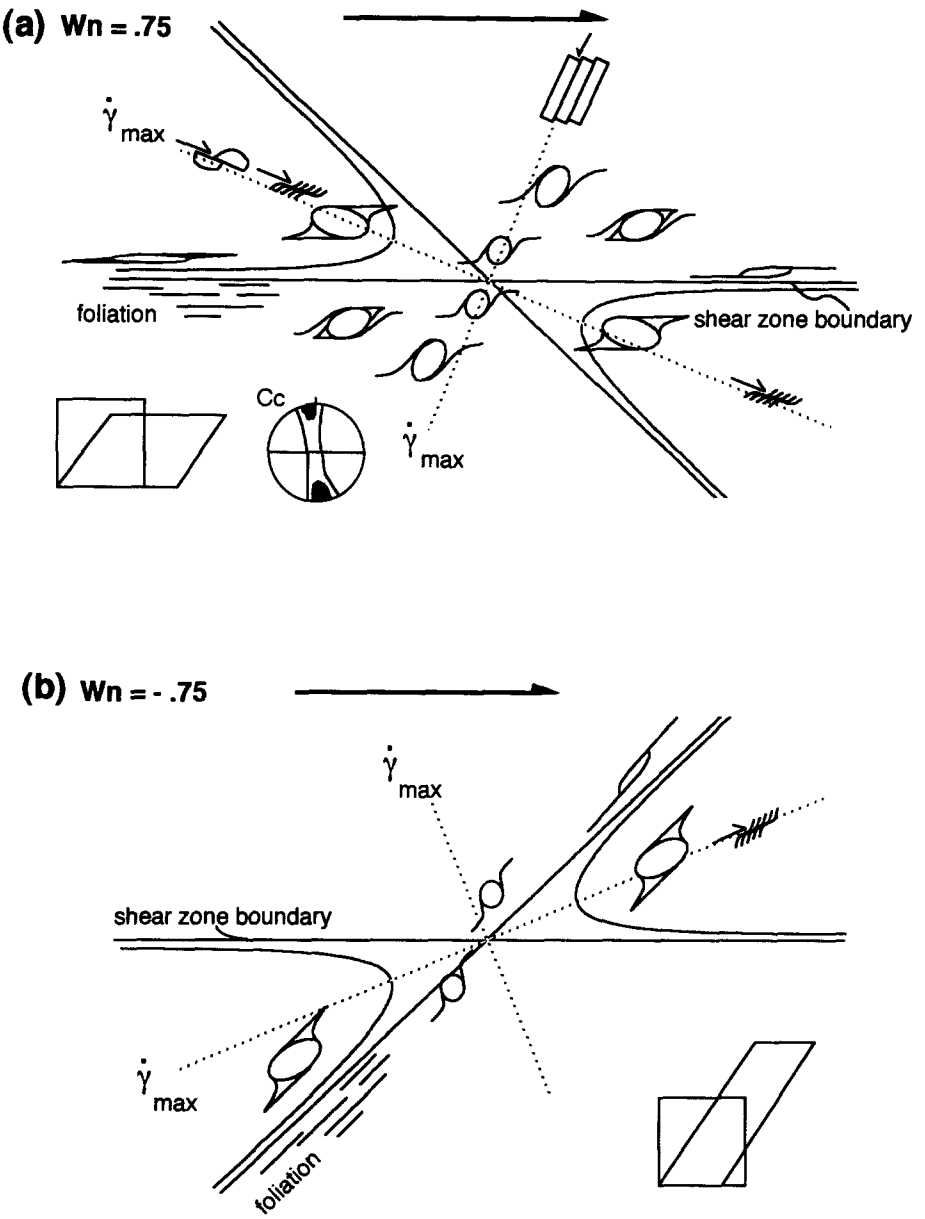

Fig. 20. Synoptic diagram of meso- and micro-scale structures in a dextral sub-simple shear zone with (a) $W_n = 0.75$ (narrowing) and (b) $W_n = -0.75$ (broadening). Cartoons represent various features in their approximate position and/or orientation on the hyperbolic net. Hyperbolae are stable ellipse orientations as in Fig. 18. Solid lines are eigenvectors, dotted lines are direction of maximum shear strain rate. See text for discussion.

orientations. If a compositionally stiffer band is parallel to the stable eigenvector (Figs. 22a–f), it may become boudinaged. Subsequent rotation of boudin fragments may be in the same sense as the shearing for brittle rigid boudinage or backward in the case of deformable fragments (see Hanmer 1986). If a rigid layer (Fig. 22a) breaks into rigid blocks (Fig. 22b), the points representing block shapes on the hyperbolic net are shifted towards the origin and thus enter the field of forward rotation (Fig. 22c). Rotations cease when block orientations again plot on the locus of stable ends. A stiff but more deformable layer (Fig. 22d) may break into deformable fragments (Fig. 22e), which then back-rotate (Fig. 22f) due to counterclockwise spin of their axes through material lines, as may be demonstrated by drawing elliptical fragment outlines on a card deck and then shearing the cards. The corresponding trajectory on the hyperbolic net is illustrated by the arrows in Fig. 22(f). If there is a planar compositional band parallel to the unstable eigenvector (Fig. 22g) then asymmetric folds may develop during shear (Fig. 22b), which may subsequently amplify into sheath folds.

Strain partitioning

Strain in shear zones is frequently partitioned into bands of intense shear and intervening lithons of less intense shear (e.g. Coward 1976, Simpson 1983, Bell 1986). Bell & Johnson (1992) and Bell *et al.* (1992 and self-references therein) have suggested that porphyroblasts within such lithons do not rotate (but see Passchier *et al.* 1992). Bell & Johnson (1992) have explained such features as δ grains by invoking a series of three different and orthogonal phases of deformation (their fig. 25), but this is refuted by the occurrence of σ and δ grains on the same flow plane. Even in pure shear, elongate grains

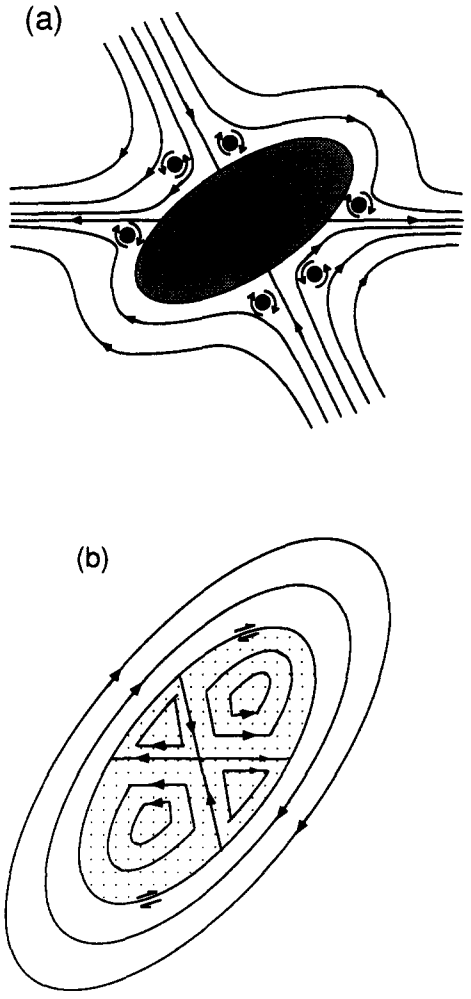

Fig. 21. (a) Disturbance of flow lines for sub-simple shear around a domain of super-simple shear such as a deformable porphyroclast in a narrowing zone. Note that trajectories represent particle paths as in Fig. 2, and not ellipses as in Fig. 18. Flow disturbance may cause back-rotation of satellite grains even if they are circular in cross section. Eigenvectors lie in planes of shear because there are different displacement rates along particle paths on either side (labelled 'faster' and 'slower'). (b) Flow lines within and around a soft grain undergoing sub simple shear in a matrix that undergoes super simple shear.

must rotate towards the principal stretch axis by an amount that depends on their axial ratio and initial orientation (Dunnet 1969, Ghosh & Ramberg 1976, Lisle 1977, 1985). In addition, three separate and orthogonal orogenic events would cause shear zone boundaries to be decidedly non-planar, and yet δ grains are most commonly found in parallel-sided ultramylonite zones. We see no reason to invoke a special cause for δ grains in thick shear zones as opposed to narrow ones, nor do we find any inconsistencies between Bell & Johnson's (1992) figs. 1–3 and 10, and a single event, general shear history.

Tectonic implications of sub-simple shear

The tectonic implications of sub-simple shear zones, whether narrowing or broadening must be carefully considered. These shear zones may occur only: (1) where the wall rocks to a high strain zone are able to deform; (2) where there is an area change in the section; (3) where the shear zone is curved or has non-parallel sides; or (4) where there is a fault between the wall rock and the sheared rock. For a straight, parallel-sided shear zone of constant cross-sectional area, simple shear is the only possible deformation regime if the wall rock remains undeformed and attached (Ramsay & Graham 1970). There are, however, several tectonic scenarios that provide the means for more general shear. Area changes may be facilitated where shear zones rise to the surface of the earth or where nappes spread, as often occurs in the internal parts of orogens. In transpression or transtension zones, material moves laterally into or out of the profile plane. In the case of extreme transpression, the maximum principal stretch may be the axis of the rotational component of deformation (Fig. 23), and a mineral lineation could develop orthogonal to the directions of tails of oblate grains (prolate grains are only transiently stable in this case; Passchier 1987). Broadening sub-simple shear zones may be distinguished by the relatively large angle between foliation and shear zone boundary, even at very high strains, and by the occurrence of dilatational structures such as intrusive sheets parallel to the boundary (Escher *et al.* 1975). Both broadening and narrowing shear zones may occur in both extensional and compressional tectonic settings. It is important to consider zone orientations relative to regional décollements before making large-scale inferences from the geometry of mesoscale general shear deformation.

CONCLUSIONS

The polar Mohr constructions presented here for finite and infinitesimal strain, flow and acceleration, are ideally suited for the analysis of general shear in high strain zones. The kinematic vorticity number W_n is readily obtainable from the angle between the eigenvectors, where one eigenvector is fixed to the flow plane of the simple shear component, and the orientation of the other depends on the pure shear contribution. Narrowing vs broadening sub-simple shear zones can be distinguished using the relationship between foliation and shear zone boundary. Super-simple shear is generally confined to the region in and around deformable porphyroclasts.

The hyperbolic net allows a simple and rapid analysis of W_n using the stable end orientations of rigid and deformable σ, δ and complex σ–δ porphyroclasts. Other kinematic indicators such as myrmekitic feldspars, mica fish, asymmetric boudinage and calcite lattice-preferred orientations are consistent with this approach. Fractures in feldspar grains and shear bands may form along the directions of maximum shear strain rate and subsequently rotate with progressive strain; if formed late in the deformation history their orientations may allow an approximation of the general shear state.

Acknowledgements—The impetus for this work began with the joint meeting of the Dutch and German Geological Societies in Bochum,

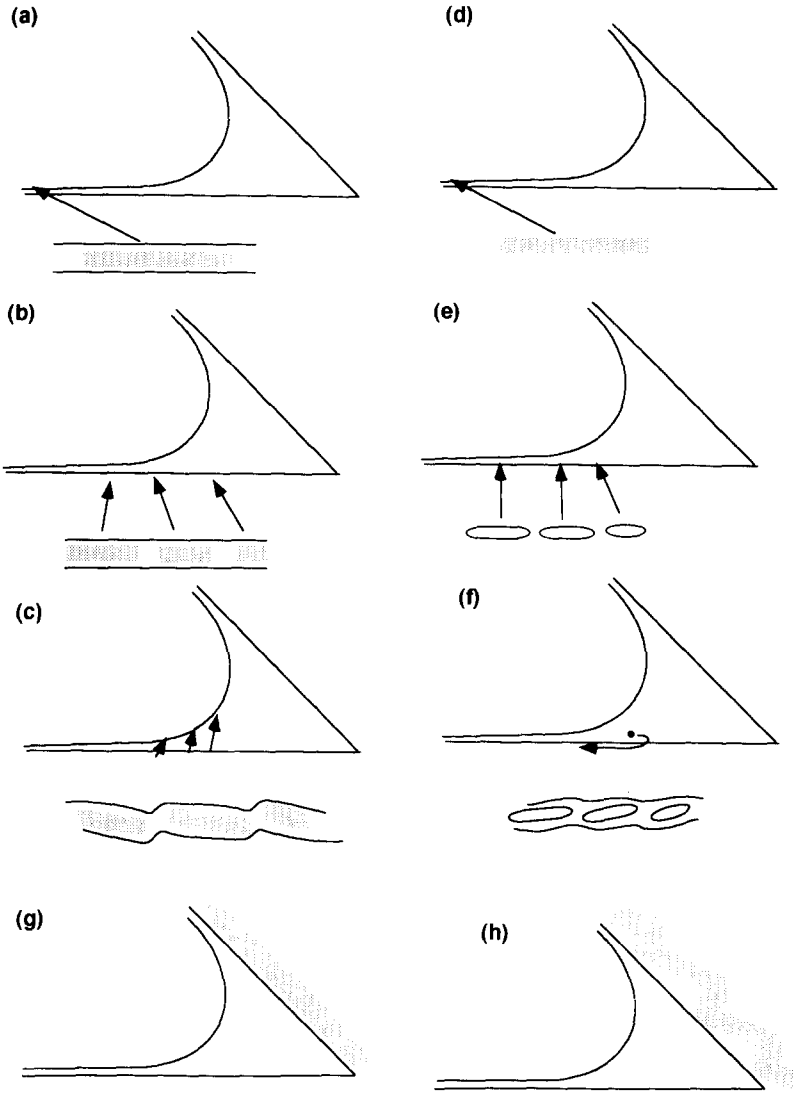

Fig. 22. Explanation of asymmetric boudinage and fold geometry in general shear zones. (a) Initial rigid layer. (b) Boudinage into rigid fragments that rotate forward (c) into stable end orientations. (d) More deformable stiff layer breaks into deformable boudins (e). (f) Deformable fragments may rotate backwards owing to spin of their axes. (g) Stiff layer oriented parallel to unstable eigenvector. (h) Individual fold axial planes are sub-parallel to the shear zone boundary.

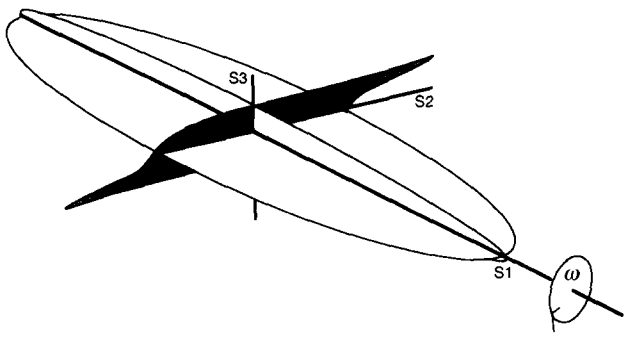

Fig. 23. Kinematic rotation axis may be parallel to S_1 in a zone of transpression.

Germany, in 1990 and was further vitalized during preparations for the 1991 Geological Society of America Structural Geology and Tectonics Division short course on Deformation and Kinematics in High Strain Zones presented by the authors in San Diego, California. The participants in the short course are thanked for their enthusiasm in putting these ideas to the test. Reviews by Chris Talbot and an anonymous reviewer were most helpful. C. Simpson acknowledges research release time from the Division of Earth Sciences, U.S. National Science Foundation.

REFERENCES

Allison, I. 1984. The pole of the Mohr diagram. *J. Struct. Geol.* **6**, 331–334.

Behrmann, J. H. 1987. A precautionary note on shear bands as kinematic indicators. *J. Struct. Geol.* **9**, 659–666.

Bell, T. H. 1986. Foliation development and refraction in metamorphic rocks: reactivation of earlier foliations and decrenulation due to shifting patterns of deformation partitioning. *J. metamorph. Geol.* **3**, 109–118.

Bell, T. H. & Johnson, S. E. 1992. Shear sense: a new approach that resolves conflicts between criteria in metamorphic rocks. *J. metamorph. Geol.* **10**, 99–124.

Bell, T. H., Johnson, S. E., Davis, B., Forde, A., Hayward, N. & Wilkins, C. 1992. Porphyroblast inclusion-trail orientation data: eppure non son girate. *J. metamorph. Geol.* **10**, 295–307.

Bobyarchick, A. R. 1986. The eigenvalues of steady state flow in Mohr space. *Tectonophysics* **122**, 35–51.

Brace, W. F. 1961. Mohr construction in the analysis of large geologic strain. *Bull. geol. Soc. Am.* **72**, 1059–1080.

Choukroune, P., Gapais, D. & Merle, O. 1987. Shear criteria and structural asymmetry. *J. Struct. Geol.* **9**, 525–530.

Coward, M. P. 1976. Strain within ductile shear zones. *Tectonophysics* **34**, 181–197.

Curie, P. 1894. Sur la symetrie dans les phénomènes physiques: symetrie d'um champ électrique et d'un champ magnétique. *J. Phys.* **3**, 393–415.

Davidson, A., Culshaw, N. G. & Nadeau, L. 1982. A tectonometamorphic framework for part of the Grenville Province, Parry Sound region. Ontario. *Geol. Surv. Can. Pap.* **82-1A**, 175–190.

Dennis, A. & Secor, D. T. 1987. A model for the development of crenulations in shear zones with applications from the Southern Appalachian Piedmont. *J. Struct. Geol.* **9**, 809–817.

De Paor, D. G. 1983. Orthographic analysis of geologic structures—I. Deformation theory. *J. Struct. Geol.* **5**, 255–278.

De Paor, D. G. 1988. R_f/ϕ_f strain analysis using an orientation net. *J. Struct. Geol.* **10**, 323–333.

de Sitter, L. U. 1956. *Structural Geology*. McGraw-Hill, New York.

Dunnet, D. 1969. A technique of finite strain analysis using elliptical particles. *Tectonophysics* **7**, 117–136.

Dunnet, D. & Siddans, A. W. B. 1971. Non-random sedimentary fabrics and their modification by strain. *Tectonophysics* **12**, 307–325.

Elliott, D. 1970. Determination of finite strain and initial shape from deformed elliptical objects. *Bull. geol. Soc. Am.* **81**, 2221–2236.

Elliott, D. 1972. Deformation paths in structural geology. *Bull geol. Soc. Am.* **83**, 2621–2638.

Escher, A., Escher, J. C. & Watterson, J. 1975. The reorientation of the Kangamuit dyke swarm, west Greenland. *Can. J. Earth Sci.* **12**, 158, 173.

Flinn, D. 1962. On folding during three dimensional progressive deformation. *Q. J. geol. Soc. Lond.* **B** 385–433.

Freeman, B. 1985. The motion of rigid ellipsoidal particles in slow flows. *Tectonophysics* **113**, 163–183.

Gay, N. C. 1968. The motion of rigid particles embedded in a viscous fluid during pure shear deformation of the fluid. *Tectonophysics* **3**, 81–88.

Ghosh, S. K. & Ramberg, H. 1976. Reorientation of inclusions by combination of pure and simple shear. *Tectonophysics* **34**, 1–70.

Hanmer, S. 1984. Structure of the junction of three tectonic slices, Ontario Gneiss segment, Grenville Province. *Geol. Surv. Can. Pap.* **84-1B**, 109–120.

Hanmer, S. 1986. Asymmetrical pull-aparts and foliation fish as kinematic indicators. *J. Struct. Geol.* **8**, 111–122.

Hanmer, S. & Passchier, C. W. 1991. Shear sense indicators: A review. *Geol. Surv. Can. Pap.* **90–117**.

Harker, A. 1995. On slaty cleavage and allied rock structures with special reference to the mechanical theories of their origin. *Rep. Br. Ass. 55th Meeting*, 1–40.

Harris, L. B. & Cobbold, P. R. 1985. Development of conjugate shear bands during bulk simple shearing. *J. Struct. Geol.* **7**, 37–44.

Jeffrey, G. B. 1923. The motion of ellipsoidal particles immersed in a viscous fluid. *Proc. R. Soc. Lond.* **A102**, 161–179.

Lisle, R. J. 1977. Estimation of tectonic strain ratio from the mean shape of deformed elliptical markers. *Geologie Mijnb.* **56**, 140–144.

Lisle, R. J. 1985. *Geological Strain Analysis: A Manual for the R_f/ϕ Technique*. Pergamon. London.

Lister, G. S. & Price, G. P. 1978. Fabric development in a quartz-feldspar mylonite. *Tectonophysics* **49**, 37–78.

Lister, G. S. & Snoke, A. W. 1984. S–C mylonites. *J. Struct. Geol.* **6**, 617–638.

Lister, G. S. & Williams, P. F. 1983. The partitioning of deformation in flowing rock masses. *Tectonophysics* **92**, 1–33.

Malavieille, J. & Ritz, J. F. 1989. Mylonitic deformation of evaporites in décollements: examples from the Southern Alps, France. *J. Struct. Geol.* **11**, 583–590.

March, A. 1932. Mathematische theorie der Regelung nach der Korngestalt. *Z. Kristallogr.* **81**, 285–297.

Matthews, P. E., Bond, R. A. B. & Van den Berg, J. J. 1974. An algebraic method of strain analysis using elliptical markers. *Tectonophysics* **24**, 31–67.

Means, W. D. 1982. An unfamiliar Mohr circle construction for finite strain. *Tectonophysics* **80**, T1–T6.

Means, W. D. 1983. Application of the Mohr-circle construction to problems of inhomogeneous deformation. *J. Struct. Geol.* **5**, 279–286.

Means, W. D., Hobbs, B. E., Lister G. S. & Williams, P. F. 1980. Vorticity and non-coaxiality in progressive deformations. *J. Struct. Geol.* **2**, 371–378.

Nadai, A. 1963. *Theory of Flow and Fracture of Solids*. McGraw-Hill, New York.

Owens, W. H. 1973. Strain modification of angular density distributions. *Tectonophysics* **16**, 249–261.

Passchier, C. W. 1986. Flow in natural shear zones—the consequences of spinning flow regimes. *Earth Planet. Sci. Lett.* **77**, 70–80.

Passchier, C. W. 1987. Stable positions of rigid objects in non-coaxial flow—a study in vorticity analysis. *J. Struct. Geol.* **9**, 679–690.

Passchier, C. W. 1988. Analysis of deformation paths in shear zones. *Geol. Rdsch.* **77**, 308–318.

Passchier, C. W. & Simpson, C. 1986. Porphyroclast systems as kinematic indicators. *J. Struct. Geol.* **8**, 831–843.

Passchier, C. W., Trouw, R. A. J., Zwart, H. J. & Vissers, R. L. M. 1992. Porphyroblast rotation: eppur si muove? *J. metamorph. Geol.* **10**, 283–294.

Platt, J. P. 1984. Secondary cleavages in ductile shear zones. *J. Struct. Geol.* **6**, 439–442.

Platt, J. P. & Vissers, R. L. M. 1980. Extensional structures in anisotropic rocks. *J. Struct. Geol.* **2**, 397–410.

Ramberg, H. 1975. Particle paths, displacement, and progressive strain applicable to rocks. *Tectonophysics* **28**, 1–37.

Ramsay, J. G. 1967. *Folding and Fracturing of Rocks*. McGraw-Hill, New York.

Ramsay, J. G. 1980. The crack–seal mechanism of rock deformation. *Nature* **284**, 135–139.

Ramsay, R. G. & Graham, R. H. 1970. Strain variations in shear belts. *Can. J. Earth Sci.* **7**, 786–813.

Ramsay, J. G. & Huber, M. I. 1987. *The Techniques of Modern Structural Geology, Volume 2: Folds and Fractures*. Academic Press, London.

Ramsay, R. G. & Wood, D. S. 1973. The geometric effects of volume change during deformation processes. *Tectonophysics*, **16**, 263–277.

Rosenfeld, J. L. 1968. Garnet rotations due to the major Paleozoic deformations in southeast Vermont. In: *Studies of Appalachian Geology: Northern and Maritime* (edited by White, W. S., Zen, E., Hadley, J. B. & Thompson, J. B). John Wiley, New York, 185–202.

Sanderson, D. J. 1976. The superposition of compaction and plane strain. *Tectonophysics* **30**, 35–54.

Sanderson, D. J. & Marchini, W. R. D. 1984. Transpression. *J. Struct. Geol.* **6**, 449–458.

Schley, H. M. 1973. *Div, Grad, Curl, And All That: An Informal Text on Vector Calculus*. W. W. Norton & Co. Inc., New York.

Schmid, S. M. & Casey, M. 1986. Complete fabric analysis of some commonly observed quartz *c*-axis patterns. *Am. Geophys. Un. Geophys. Monogr.* **36**, 263–286.

Schoneveld, C. 1977. A study of some typical inclusion patterns in strongly paracrystalline rotated garnets. *Tectonophysics* **39**, 453–471.

Simpson, C. 1983. Displacement and strain patterns from naturally occurring shear zone terminations. *J. Struct. Geol.* **5**, 497–506.

Simpson, C. & Schmid, S. M. 1983. An evaluation of criteria to determine the sense of movement in sheared rocks. *Bull. geol. Soc. Am.* **94**, 1281–1288.

Simpson, C. & Wintsch, R. P. 1986. Evidence for deformation-induced K-feldspar replacement by myrmekite. *J. metamorph. Geol.* **7**, 261–275.

Sorby, H. C. 1855. On slaty cleavage as exhibited in the Devonian limestones of Devonshire. *Phil. Mag.* **11**, 20–37.

Takagi, H. & Ito, M. 1988. The use of asymmetric pressure shadows in mylonites to determine the sense of shear. *J. Struct. Geol.* **10**, 347–360.

Talbot, C. J., 1970. The minimum strain ellipsoid using quartz veins. *Tectonophysics* **9**, 47–76.

Talbot, C. J. & Jackson, M. A. 1987. Internal kinematics of salt diapirs. *Bull. Am. Ass. Petrol. Geol.* **71**, 1068–1098.

Truesdell, C. 1954. *The Kinematics of Vorticity*. Indiana University Press, Bloomington.

Urai, J. L., Williams, P. F. & van Roermund, H. L. M. 1991. Kinematics of crystal growth in syntectonic fibrous veins. *J. Struct. Geol.* **13**, 823–836.

Vissers, R. L. M. 1987. The effect of foliation orientation on the inferred rotation axes and rotation angles of rotated porphyroblasts. *Tectonophysics* **139**, 275–283.

Vissers, R. L. M. 1989. Asymmetric *c*-axis fabrics and flow vorticity: a study using rotated garnets. *J. Struct. Geol.* **11**, 231–244.

Weijermars, R. 1991. The role of stress in ductile deformation. *J. Struct. Geol.* **13**, 1061–1078.

Weijermars, R. & Rondeel, H. E. 1984. Shear band foliation as indicator of sense of shear: field observations in central Spain. *Geology* **12**, 603–606.

Wenk, H.-R., Takeshita, T., Bechler, E., Erskine, B. G. & Matthies, S. 1987. Pure shear and simple shear calcite textures. Comparison of experimental, theoretical and natural data. *J. Struct. Geol.* **9**, 731–745.

Wettstein, A. 1886. Über die Fischfauna des Tertiären Glarner Schiefers. *Schweiz. Paläont. Ges. Abh.* **13**, 1–101.

APPENDIX

Passchier (1987) gives the following formula for the stable end position of a rigid elongate porphyroclast, in a general shear zone in which the pure shear component acts to narrow the zone:

$$\eta = (1/2)\sin^{-1}\{(W_n/B)[\sqrt{(1-W_n^2)} \pm \sqrt{(B^2 - W_n^2)}]\}, \quad \text{(A1)}$$

where B is the shape factor, and η is the orientation of the long axis of the grain (Fig. A1).

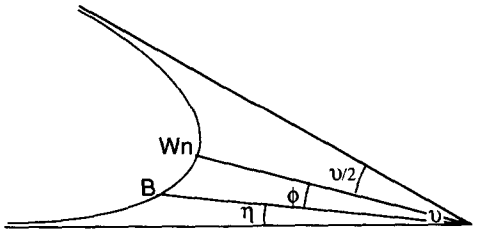

Fig. A1. Demonstration that stable end orientations plot on a curve from the hyperbolic net by showing that equation (11) of this paper is equivalent to Appendix equation (A1). ν is the angle between asymptotes, W_n is apical value of radius vector B which is related to ellipse axial ratio R and shape factor E by equations (12a) and (12b). ϕ is the angular measure used in this paper. Passchier (1987) uses the alternative angle η.

Translating equation (A20) of De Paor (1988) using the identity

$$B = \tanh(2E), \quad \text{(A2)}$$

we propose that the polar equation of the hyperbola in Fig. A1 is,

$$B = W_n/\cos 2\phi, \quad (11)$$

where the kinematic vorticity number W_n is the value of B at the apex and also the cosine of the angle between the asymptotes,

$$W_n = \cos(\nu). \quad \text{(A3)}$$

The following derivation demonstrates that equation (11) of this paper is equivalent to equation (A1) above and provides an easier way to calculate W_n. Note the different sense in which angles are measured in the paper (Fig. A1) vs Passchier (1987).

From equation (11), substituting for 2ϕ,

$$W_n/B = \cos(\nu - 2\eta) \quad \text{(A4)}$$

$$= \cos\nu\cos 2\eta + \sin\nu\sin 2\eta \quad \text{(A5)}$$

$$= W_n\cos 2\eta + \sin\nu\sin 2\eta. \quad \text{(A6)}$$

Rearranging, and then squaring both sides,

$$W_n\cos 2\eta = W_n/B - \sin\nu\sin 2\eta \quad \text{(A7)}$$

$$W_n^2(1-\sin^2 2\eta) = W_n^2/B^2 - (2W_n/B)\sin\nu\sin 2\eta + (1-W_n^2)\sin^2 2\eta \quad \text{(A8)}$$

$$0 = W_n((1/B)-B) - 2\sin\nu\sin 2\eta + (B/W_n)\sin^2 2\eta. \quad \text{(A9)}$$

Solving this quadratic,

$$\sin 2\eta = [2\sin\nu \pm \sqrt{(4\sin^2\nu - 4(1-B^2))}]/(2B/W_n) \quad \text{(A10)}$$

$$= (W_n/B)[\sqrt{(1-W_n^2)} \pm \sqrt{\{(1-W_n^2)-(1-B^2)\}}] \quad \text{(A11)}$$

or

$$\eta = (1/2)\sin^{-1}\{(W_n/B)[\sqrt{(1-W_n^2)} \pm \sqrt{(B^2-W_n^2)}]\}. \quad \text{(A1)}$$